703

CHARACTERIZATION OF OPTICAL FIBERS AND CABLES

OPTICAL AND MECHANICAL CHARACTERIZATION

OF

OPTICAL FIBERS AND FIBER CABLES

by

ANDREW CLAUDE CERVIN, B.Sc.

A Project

Submitted to the School of Graduate Studies

in Partial Fulfilment of the Requirements

of the Degree

Master of Engineering

McMaster University

1980

MASTER OF ENGINEERING — McMaster University

(Engineering Physics) — Hamilton, Ontario

Title: Optical and Mechanical Characterization of Optical Fibers and Cables Part B

Author: Andrew Claude Cervin, B.Sc. (University of Windsor)

Supervisor: Dr. K. Abe, Bell-Northern Research, Ottawa, Ontario

Number of pages: vii, 59

ABSTRACT

This paper describes optical fiber and cable evaluation carried out at Bell-Northern Research during the summer period of May-August, 1980. Contemporary fibers and cables designed for telecommunications use were evaluated and the results on the following three areas are reported:

(1) Resistance of fiber optics cables to temperature extremes and mechanical abuse.

(2) Fiber tensile strength, both fast-fracture and fatigue, and a test method to predict longevity of the fibers.

(3) Pulse broadening, measured as a function of link lengths in order to establish engineering rules which can predict performance for 10 km lengths (typical repeater spacing) from the individual fiber characteristics.

ACKNOWLEDGEMENTS

I am very grateful to Dr. Koichi Abe for his help and support during my term at Bell-Northern Research. I also thank Bell-Northern Research for providing the opportunity to work there.

Thanks to Glen Dack, Sam Yutaki, and Felix Kapron for many useful discussions and to Don Kneller for doing the computer plots of pulse broadening.

I am grateful to L. Labuda and Janet Arsenault for the typing of this project.

I would like to thank my parents for much help and support.

The work was done under an NSERC postgraduate scholarship. I thank NSERC for the award and for the fine service they provided during the period of the award.

TABLE OF CONTENTS

LIST OF TABLES AND FIGURES

CHAPTER 1

INTRODUCTION

The design of fiber optics communications systems is still a new and uncertain task. The components of the systems are not yet well-characterized or understood; their behaviour in the field is still in the testing stage. This report is part of on-going research into the characteristics of various aspects of the transmission medium, i.e., the fibers and fiber cables. The requirements for communications equipment are rigorous, the life of the cables must reach twenty years with no failures and minimal degradation of performance. Copper cables are well-understood, and do last this long, but fiber cables are new and perform differently. The fibers must be protected from stresses and crushing forces, water and installation forces while still retaining their desirable features: high bandwidth, low weight, small size, etc. The cable design described in Chapter 1 meets these requirements. Chapter 1 also describes the behaviour of these cables with variations in temperature, mechanical forces, and water penetration of the jacket (ice crush test).

In Chapter 3 the mechanical strength of fibers is studied. The difficulties in predicting the strength of kilometers of fibers and testing for fibers that will last many years are detailed. A method of testing fibers in manufacturing is presented.

Chapter 4 shows the effect on bandwidth of splicing many lengths of fiber together in a long link. The resulting bandwidth is better than would be expected from the individual bandwidths of the fibers. The intention was to gather more data to refine the engineering rules for predicting the bandwidth of concatenated fibers. The fibers used were from several different manufacturers and of recent design.

The work done here is obviously incomplete. The time available did not allow the full scope of reliability and aging tests to be carried out. Thus only a small part can be presented of the total work required. Other tests must be done as well: attenuation versus tension, static fatigue (already started), attenuation versus tension in the cable, prolonged aging of cables at high temperatures, etc. Empirical data is needed for these in order to give the system designer enough information to make appropriate choice of components. If such information is not available then generous safety margins must be used in the design to insure sufficient reliability in performance.

CHAPTER 2

CABLE DESIGN AND TESTING FOR FIBER OPTICS COMMUNICATIONS

2.1 Cable Design

The components of a communications system must meet stringent requirements. Extremes of temperature must be borne with little or no degradation of performance. Cables are expected to last twenty years or more before replacement in normal service. For fiber optics cables, the glass fibers must not have drastic long term attenuation increase under field conditions. The cable must also protect the fibers from rigors of installation where they are pulled through underground ducts, impacted by hammers, crushed by trucks, etc.

The cable design[1] tested here achieves the protection goals and most of the attenuation requirements over the operating temperature range. The cable has a central steel strength member around which a polyethylene core is extruded. Slots milled in the core hold the fibers and prevent any crush force from damaging the fibers. The slots are spiralled around the core, reversing every six inches or so, to reduce bending effects. The fibers and/or PIC twisted pairs (copper wire) are laid into the slots and held by a double wrapping of mylar tape. This cable core is further wrapped with solid mylar and aluminum tapes. A black polyethylene sheath is extruded on top. Cables of this design are capable of

holding thirty-six fibers.

Variations can be made to the basic design; a filling material can be used when the core and the aluminum tape to stop water ingress; additional armour can be wrapped over the sheath, etc. Fig. 2.1 shows a cross-section of the basic cable. The prototype filled cables were tested to evaluate the various filling components. Silicone grease and Dri-Fill powder were used for the prototype cables.

2.2 Detailed Requirements for Optical Communications Cables[2]

The operational temperature range of cables is from -40° to $+60^{\circ}$C. Over this range the attenuation shall not increase more than 25%. The following tests must not induce more than .05 dB/Km attenuation increase: 9 impacts of a 750 gm. hammer with a 25 mm diameter head falling from 1.1 meter height, crushing over a 25 cm length of the cable with 30 kN force for 10 min., flexing $\pm$ 90° between two mandrels with the diameter of 10 times the diameter of the cable (flex rate of 25 cycles per min.), and bending the cable 10 turns around a mandrel of the same size and holding for 10 minutes.

The cables are rated for a tensile force of 700 lbs. during installation in underground ducts. Therefore, tension testing is necessary on a representative length of cable. The cable must withstand tension up to 1200 lbs. in 4 steps. Each step is to be held for 30 min., then relaxed for another 30 min. Readings

should be taken at the beginning and end of each half hour.

In order to simulate cable puncture followed by water ingress a 7 mm hole is to be drilled in the sheath and a 1 meter head of water applied to it. Several of these "crush points" spaced with 50 meter intervals are to be installed. The cable is then to be temperature cycled between $+25^{\circ}$ and $-10^{\circ}C$, simulating freezing temperatures in the field.

2.3 Test Method

Temperature testing of the cable was done with a Coldstream environmental testing chamber. This gave a temperature range between $+75^{\circ}$ to $-50^{\circ}C$. The cable was wound loosely on a rack by hand. The appoximate diameter of the resulting loops was about 6 ft. The large diameter of the loops minimized the effects of bending.

The light sources were two Burrus-type LED's, emitting light from approximately 840 nm wavelength. They were connected in series and powered by a Keithley current source at 100 mA. The light output was fed into a four-way splitter. Each output of the splitter fed into a detector to monitor fluctuations in the LED output power. The detectors were solar cells in lightproof metal cans. The solar cells gave a current proportional to incident light power. Other outputs of the splitter were spliced to the fibers in the cable. Two fibers from each slot were tested. Six more detectors were used for monitoring the cable output. Two

cables were tested at the same time. A Keithley picoammeter measured the current from the solar cells. A block diagram of the experimental setup is shown in Fig. 2.3.

Temperature in the chamber was measured by five thermocouples distributed inside the chamber; some were in intimate contact with the cable, and others in the air. The tempeprature was changed approximately 20°C for each step. When the five thermocouples showed the same temperature for at least one hour, it was assumed the cable had reached equilibrium and a measurement was taken.

To simulate cable puncture and water ingress, holes were drilled (carefully) through the outer sheath and aluminum tape to expose the core. A standpipe was put around this (Fig. 2.2) sealed with rubber tape and filled with water. For this test a temperature range from +25° to -10°C was used. A buried cable would not see the full operational temperature range described previously or else (aerial cables for example) it would not see the 1 meter head of water. In spite of this, a full range check was done to see if the cable suffered any catastrophic attenuation increase.

Impact tests were done with a hammer of specific cross section and weight dropped from a height of 1.1 meters guided down the inside of a tube. The cable was moved after three impacts in order to hit all sides of the spiral around the core.

Tensile testing was done on a 500 meter section of

prototype cable as specified in Section 2.2. Steel cables clamped to the core, and taped to the jacket as well, provided the means to grip the cable. A come-along was used to tension the cable. Attenuation was monitored throughout the pulls in the same way as for the temperature tests. A load cell gave the tensile force readings. Four pull tests were performed with tensile force levels of 505, 760, 915 and 1080 lbs.

2.4 Test Results

Five different types of cable were used for the tests:

1. Cable 1: no filling at all, for use in a pressurized system.
2. Cable 2: silicone grease filling.
3. Cables 3 and 4: different makes of fibers but the same Dri=Fill power filling.
4. Cable 5: powder-filled, with gopher-tape armour and an extra polyethylene jacket.

Temperature cycling was done on all the cables; mechanical tests were done on Cables 1 and 4. Pull and some mechanical testing was done on Cable 3.

Attenuation increases at the ends of the temperature range (observed in the graphs) were caused by stress in the fibers produced by the differing expansion coefficients of the cable materials. The graphs show changes in attenuation relative to mean temperature. Negative signs indicate that attenuation for

the cable has decreased.

Figures 2.4 a, b, c, d, and e show similar trends and equivalent values of maximum attenuation increase. Figure 2.4 b, the grease-filled cable, shows a catastrophic increase at low temperatures. Hysteresis is apparent if the cycle is traced through, i.e., the attenuation remains high until $-35^{\circ}C$ is exceeded on the increasing part of the cycle, but is lower on the decreasing part of the cycle. This was found[3] to be caused by crystallization of the grease at $-40^{\circ}C$, placing excessive stress on the fibers. Crystallization was not reversed until a temperature of $-35^{\circ}C$ was reached, resulting in high attenuation up to that point. Longer stabilization at -35° would reduce this effect but required too much time.

Cables 1, 3, 4 and 5 had acceptable increases over the full temperature range (initial attenuation of 3 dB/km allows .75 dB/km increase). The worst fiber in the gopher tape cable exceeded this but futher tests showed that fiber to be anomalous; other fibers in the cable behaved more like the first two.

A short length reading was taken on the gopher tape cable to measure the total attenuation. This proved to be about double the specified attenuation. A pigtail (500 m of fiber), scrambled the modes and improved the launching condition. This test method gave agreement with original measurement of the cable attenuation within .02 dB/km. Temperature cycling was continued with the pigtails to see if the results were affected. Changes in

attenuation were less with the pigtails than without. Since all the other tests were done without pigtails, the cable performance should actually be better than shown in Fig. 2.4.

Mechanical tests done on Cable 1 had no optical effect at all. All these tests were done at a temperature of 25°C. Impact testing caused visible damage.

Table 2.1 shows results of the ice crush test on Cable 4. The cable is highly resistant to water pentration, tests show 10-15 inches at most. The significant increase (1.4 db), occurs at -37°C, an uncommon temperature for most underground cables. Compensation for cable attenuation at the various temperatures was done with values from Fig. 2.3 d. With six standpipes spaced at 50 m intervals the highest attenuation at -10°C was .8 db.

Mechanical tests done on Cable 3 showed no effect whatsoever.

Pull test results, shown in Table 2.2, gave varied results for the different fibers in the cable. Attenuation first increased, then recovered slowly during the half hour under tension, except in one case: fiber B during the 1080 lb pull. Upon release attenuation did not recover completely to its starting value, though in some cases it was better later. Attenuation decreased during the half hour relaxed, except in one case: fiber G after the 760 lb pull. All fibers benefitted in the end from the tension, showing less attenuation than at the start. The attenuation increase at the end of the half-hour

relase, following the 760 lb pull, is not drastic and would, in all probability, decrease still further.

The ice crush test on Cable 5 shows even less increase than for Cable 4. With cable attenuation included, only 1 dB increases is observed with four standpipes at $-40^{o}C$. Left overnight at this temperature the cable recovered to .9 dB. Corrected for cable attenuation a .8 dB increase with four standpipes is obtained.

2.5 Conclusions

These tests show that powder filling is the best filling for cables. The grease filled cable has high attenuation at low temperatures. This could be solved by using a different, lower temperature grease, which would be much more costly. Powder is cheap and effective. Water is effectively stopped from penetrating the cable and optical properties are unimpaired. Questions arise as to whether the powder would remain uniformly distributed around the core under the vibrations caused by shipping and possible aerial cable "dancing". Tests should be made to observe the effects of such vibrations on the distribution of powder around the core.

Mechanical properties of the cables are very good. The specifications and, indeed, the requirements are met and/or exceeded in all cases. Once installed the fibers should relax and even out local stresses, yielding slightly lower attenuation values.

CHAPTER 3

MECHANICAL PROPERTIES OF FIBERS

3.1 Introduction

The previous tests for the cables have been for short-term attenuation increase. The lifetime of the fibers in the cables must be predictable in order for useful communications cables to be made. Thus, failure and fatigue mechanisms in optical fibers must be understood and a method of testing must be devised to yield acceptable failure probability after twenty years in the field.

The stresses applied to the fiber during manufacturing and installation are mainly short-term. Once in service the fiber undergoes long-term (and slowly varying) stresses less than the short-term stresses experienced during manufacture. Thus both short-term (fast-fracture) and long-term (fatigue) strength of fibers must be characterized.

3.2 Basic Theory of Fast-Fracture and Fatigue Strength

Pristine, pure glass fibers are very strong: theoretical values of 20 GPa have been predicted from surface energy studies.[6] Values close to this (16 GPa) have been reported for short gauge lengths.[6] Reasons for failure at lower tensions are surface flaws and impurities. Flaws concentrate the stresses at

their tip to much greater than the average stress over the cross-section of the fiber, resulting in failure, or growth of the flaw. Evidence suggests[6] that flaw growth proceeds only in an active environment, i.e., water or wind. (OH^- ions are most active).

The analysis of fiber strength is based upon a weakest-link model. The fiber fails when the strength of the weakest section in that fiber is exceeded by the applied stress. The weakest section is the place of the largest flaw.

The difficulty in obtaining information about fiber strength is that flaw size distribution cannot be determined directly, statistical methods must be used. Kilometer lengths of fiber are not practical to test, so measurements must be done on short (< 20 m) lengths. It has been shown that extrapolation of short-length data to long lengths is unreliable.

Short length data is described by Weibull statistics[6]:

$$F(\sigma,L) = 1 - e^{\left[\left(\frac{\sigma}{\sigma_o}\right)^m\left(\frac{L}{L_o}\right)\right]}$$

where

F is the failure probability,

σ is the applied stress, and

m, σ_o, L_o are constants to be determined for each fiber.

It appears from $F(\sigma,L)$ that to extrapolate to long lengths one has only to determine m, σ_o, L_o from short length measurements and extend the graph. One difficulty with this is immediately apparent from short-length graphs (Fig.s 3.1 - 3.7).

Slope (m) changes both with length and with σ, indicating that different flaw distributions exist. It is this multimodal behaviour that makes extrapolation to long lengths or low tensions unreliable.

This multimode behaviour can be all but eliminated by very careful manufacturing processes. High-quality initial glass tubes, fire-polishing of the preform, clean room conditions, and laser-drawing are some techniques to reduce the variation in m. These methods are costly and time-consuming and are not yet feasible in mass production.

The work done on long lengths shows the difficulty in extrapolation.[6] There is little correlation between long and short length data.

There is a technique of testing that will give, if properly done, guaranteed maximum flaw sizes. This consists of applying, during manufacture, a constant controlled tension to the fiber over a short length (usually < 10 cm). Testing is continuous as the fiber is drawn. Any flaw with a critical depth greater than or equal to the critical depth that would fail under the test stress will fail. In this way, assuming no degradation of fiber strength by the proof-test, the size of the flaws can be guaranteed to be less than the size of flaws which would fail during the proof test.

The proof-test tension must be carefully chosen; it must be low enough so that rejection rates are not excessive and fiber

strength is not degraded, yet high enough so that cable manufacturing stresses can be survived and a reasonable lifetime can be guaranteed.

The fatigue of fibers under less than critical tension must be understood to give lifetime predictions for a given flaw depth and applied stress.

Fracture mechanics gives an elegant description. The fast-fracture strength of a flaw of depth a is given by the Griffith relation[6]:

$$\sigma_{1c} = \frac{.8\ k_{1c}}{\sqrt{a}}$$

k_{1c} = critical stress intensity factor and is material dependent.

For stresses less than k_{1c} we get the stress intensity factor for stress σ_1:

$$k_1 = 1.25 \sqrt{a}\ \sigma_1$$

or

$$a = \frac{.64\ k_1^2}{\sigma_1}$$

From this we calculate[6] da/dt or rate of growth of flaw under constant stress σ_1:

$$da/dt = v = \frac{1.24}{(\sigma_1)^2} \left(k_1 \frac{dk_1}{dt}\right)$$

Integrating we get t_f (time-to-failure)

$$\int_0^{t_f} dt = \frac{1.28}{\sigma_1^2} \int_{k_{1o}}^{k_{1c}} \frac{k_1}{v}\, dk_1$$

To solve this integral we need the functional dependence of k_1 on v. Two relations have been shown to work (for short lengths at least).

$$v = Ak_1^n \quad \text{(power law)}$$

$$k_1 = \alpha + \beta \ln(v) \quad \text{or:} \quad v = e^{\left(\frac{k_1 - \alpha}{\beta}\right)}$$

The short length data fit both of these well but when one extrapolates to long lengths the exponential dependance gives a shorter lifetime. This is the relation that must be used until a better relation is found. Doing the integration, assuming $k_1 << k_{1c}$ and noting that for a given flaw

$$\frac{k_1}{\sigma_1} = \frac{k_{1c}}{\sigma_{1c}}$$

we get

$$t_f = \frac{C_4}{\sigma_1^2}\, e^{-\sigma_1 C_5} [C_5 \sigma_1 + 1]$$

$$C_4 = 1.28\, \beta^2\, e^{\alpha/\beta}$$

$$C_5 = k_{1c}/\sigma_{1c}\, \beta$$

This equation is very useful because the constants can be determined without reference to particular fiber; and α and β are material/environmentally dependent, k_{1c} is a material constant,

σ_1 can be guaranteed from proof testing. Thus for a given σ one can predict with confidence (assuming good values for the constants) the lifetime of the fiber.

The environmental dependance of the lifetime has been shown to be caused mostly by water vapour.[6] There is no flaw growth in dry environments or at low temperatures, i.e. vacuum, liquid nitrogen, etc. Therefore in order to test the inert strength one must do it in such an environment.

Also, though there is disagreement, there appears to be a lower limit to the stress at which fatigue occurs. This is said to be about .15 to .25 of inert strength. As yet this is unpredictable and cannot be relied upon to yield unbroken fibers.

Now proof testing can be discussed. Requirements are that a) no damage be done to the fiber (no fatigue, no mechanical damage), and b) the σ_1 must guarantee an adequate lifetime.

Results obtained from various kinds of coatings on the surfaces of glass fibers show that there is little or no damage to the fiber from contact with rollers, wheels, etc.

Crack growth during proof testing has been calculated to be[6]:

$$\sigma_g = \sigma_p \left[1 - \left(\frac{n-2}{n+1}\right) \frac{AK^2 k_1^{n-2} \sigma_p^3}{2\dot{\sigma}_u}\right]^{\frac{1}{n-1}}$$

σ_g = guaranteed inert strength after proof testing

$\dot{\sigma}_u$ = unloading rate after stress is applied

n = power in power model of crack velocity

σ_p = proof test stress

Y = 1.25

Thus, σ_{1c} can be calculated from t_f required and σ_p can be calculated from above ($\sigma_g = \sigma_{1c}$). The requirement that σ_g be greater than instantaneous tensions during manufacturing must be met. If this is shown to fatigue fibers, lower stresses must be designed for in cabling process. It is obvious that to have confidence in lifetime predictions the material parameters must be determined reliably and accurately.

3.3 Flaw Size Reduction and Proof-Testing

Having determined that the distribution of large flaws determines the fiber strength, the question arises: How can the size and number of flaws be reduced? To answer this, the manufacturing process should be understood.

The start of a fiber is a glass tube, preferably high quality fused quartz. Both surface and bulk purity are important because in drawing the fiber the surface area of the rod is increased by around 50 times. The tube is placed on a lathe and soot from gases deposited on the wall, usually by heating with a flame. The refractive index of the soot is controlled by the flow of gases and the ratio of mixtures. The parabolic index is stepwise approximated. After deposition of soot, the tube is

collapsed into a solid rod, called a perform, by heating it further.

The preform is now ready to be drawn into fiber. Heated by a furnace, the fiber is continuously drawn from the preform. Coating of the fiber with a suitable polymer compound is done as soon after the exit of the furnace as possible. A diameter monitoring device is placed at the exit of the furnace. Pulling and proof-testing are usually done by the same device.

Flaws can be introduced at any stage. The glass tube can have impurities and surface flaws. Dusty air can produce surface flaws on the hot fiber as it exists from the furnace,[7] the fiber can be scuffled or damaged by the pulleys and coating devices.

Work has been done on determining the cause of flaws. Fire-polishing of the preform helps to reduce the number of large flaws. A big improvement was seen in changing the resistance furnace to a CO_2 laser. Apparently, the hot metal and carbon surfaces contaminated the fiber. Almost identical results were obtained with a special induction furnace.

Mechanical damage through pulleys, etc., does not have a significant effect on the strength of coated fiber; uncoated fiber is very susceptivle to damage.

The repeatability of results depends heavily on the control of all inputs to the drawing stage. The laser drawn fire-polished fibers have high, long length strength and repeatability, but are not yet feasible for commercial

production. Uncertainty in the repeatability of results again necessitates the use of proof testing.

3.4 Method of Tensile-Testing Fibers

The tensile testing was done on an Instron strain machine with a strain rate 2.5 mm/sec. Gauge length is 50 cm. Clamping of the fiber at each end was done by wrapping the fiber two-three times around the edge of a spirally slotted disk and taping the end. The slot and tape provided enough friction to pull the fiber. Breakages of the fiber in the windings were eliminated from the data.

The static fatigue was performed on 250 cm gauge length. Clamping effects were eliminated by winding the fiber around a plastic spool and taping it. The weight was hung on a wire and wrapped around the spool. The upper spool was fixed.

The Weibull plots are plots of strength (measured in Kg.) versus

$$\ln \{\ln (\frac{1}{1-P(\sigma)})\}$$

where $P(\sigma)$ is the probability that a fiber will break at a given stress. This unusual plot is obtained from the Weibull probability:

$$P(\sigma) = 1 - e^{-k(\sigma/\sigma o)}$$

where

$k = L./L_o$, and

$L.$ = gauge length.

$$\therefore \quad \left(\frac{\sigma}{\sigma o}\right)^{m} = \ln \frac{1}{1-P(\sigma)}$$

and

$$\ln \sigma = \frac{A}{m} \ln \left\{\ln\left(\frac{1}{1-P(\sigma)}\right)\right\}$$

where

A = some constant

ln = $\log_c$.

Thus plotting σ vs. $P(\sigma)$ on the special graph paper should give a straight line of slope 1/m. The value of m depends on the flaw distribution, thus a single slope on the Weibull plot indicates one distribution of flaws, i.e., a unimodal plot. If the slope changes at a certain value of σ this indicates that the flaw distribution changes at size of flaw (related to σ by Griffith relation). This would be a bimodal plot.

Aging of the fibers was accomplished by baking the fibers, wound on a drum (not tension-released), in an oven at 80°C for the specified time. They were then stress-released), in an oven at 80°C for the specified time. They were then stress-tested in the normal manner. The data is displayed on a Weibull graph.

Effects on strength of aging for various lengths of time at 80°C are shown for two fibers.

3.5 Results of Tensile Tests on Various Fibers

Plots are basically bimodal with a large increase in slope and thus m (in Weibull distribution) occurring between 5 and 6 kg

(for most of the fibers). This shows that different distribution of flaws occur, or more succinctly, the distribution of flaws does not follow the Weibull distribution.

Fiber 1, in Fig. 3.1, has a nearly unimodal plot, but is quite weak, the 100% breakage coming at only 5.2 kg. The median breaking strength (50% breakage) is 2.75 kg. The low strength was caused by the coating[8]; the coating was not uniform or thick enough.

Fiber 2, in Fig. 3.2, has more of a bimodal nature but the small hump between 5 and 6 kg indicates some differences from strict Weibull distribution in that range of flaw sizes. Median breakage is at 5.3 kg, almost twice the previous fiber's value. This fiber was coated by a well-developed process. Presence of a hump at 5 kg shows the difficulty in extrapolating to longer lengths because of the uncertainty in m.

Fiber 3, in Fig. 3.3, exhibits very nice bimodal behaviour with well-defined slopes. This fiber has a different coating from the others tested. The coating is UV cured resulting in a hard, thin coating that yields more consistent results than the softer, thicker coating on the other fibers. This fiber has been tension-released and rewound one or two times so this may be the reason for the number of large flaws. 50% breakage occurs at 5.8 kg.

The next fiber (Fig. 3.4) has the soft coating and is very weak; 50% breakage at 1.5 kg. The plot is trimodal with a very

low maximum of 4.3 kg. Some dust or contamination may have adhered to the fiber before it was coated.

Figure 3.5, (fiber from the same manufacturer as 4) shows the best characteristics of the lot, well-defined lines and very few large flaws. 50% breakage is at 6.3 kg. The variability of results with this same manufacturing process shows that not all manufacturing parameters are under control.

The aging results with regard to strength were inconclusive. The first fiber got marginally worse: 50% breakage from 6.2 to 6.1 kg, large flaws increasing slightly; lowest breakage from 2.4 to 2.2 kg, but the basic shape of the curve remaining the same. The second aged fiber shows dramatic improvement throughout: 50% breakage from 5.6 to 6.2 and a reduction in large flaws. The large flaws may have been annealled out. This is in line with other findings that have shown up to 30% increases in strength.

3.6 Conclusions

In conclusion, experimental evidence obtained here and elsewhere[6] shows that extrapolation from the data obtained in short gauge length stress measurement is not reliable as an indicator of long length strength. A better way to predict long length and low stress level failure probability and to estimate fiber lifetime is via proof testing.

Weibull plots presented here are for the purpose of

testing and comparing the process on material dependent tensile strengths.

The economics of manufacture of cables depends on the requirements of low fiber breakage versus sophistication of cabling equipment. Costs must be balanced out for an optimal solution to the problem.

CHAPTER 4

STUDIES OF PULSE BROADENING IN CONCATENATED FIBERS

4.1 Introduction

One of the most important parameters in designing an optical fiber communications system is the bandwidth or pulse broadening. This is mainly limited by the modal dispersion of the fiber, if a monochromatic light source, such as a laser, is used. It has been observed that when fibers are spliced together in long (over 3 km) lengths the pulse broadening increases less than expected from a linear addition of the individual pulse broadening of the fibers. No studies have been done on the exact mechanism for this, but the work done up until now indicates that the mode mixing due to splices and the fiber itself is causing this effect. This has great significance in the cost of fiber optics system because lower-bandwidth, and hence costly, fibers can be used to give the required performance by taking advantage of the non-linear increase of the pulse broadening. The object of this study is to deduce engineering rules to correlate the link performance (typically 10 km) with individual fiber characteristics. Concatenated attenuation measurements were performed for the same reason, i.e. prediction of link attenuation from individual fiber attenuation.

4.2 Method and Analysis

Two wavelengths were used for measuring the concatenated pulse broadenings: .9 and 1.3 μm. Pulse width (FWHM) for the .9 μm laser was .5 n sec and for 1.3 μm laser 1.2-1.3 n sec. The width was determined by the amplifier in the system (laser pulse ∿100 p sec, detector risetime ∿300 p sec). Optimum bias voltage for the .9 μm laser was about 90 V while the 1.3 μm laser required 15 V. Different avalanche photodiodes (APD's) were used for each wavelength. The Si APD for the 0.9 μm range needed up to -15 V bias and the Ge APD, for 1.3 μm range, +40 V bias. Output pulses were displayed on a sampling scope. A signal-averaging oscilloscope had to be used when the signal power level was low. This occurred at 1.3 μm, because the laser had less output. A pulse delay was used to trigger the scope. Fibers were would on tension-releasing drums to eliminate anomalous attenuation and dispersions from microbends. Splicing was done with an electric arc fusion splicer. Joints were not optimized for loss or dispersion but a visual check was done to ensure a smooth, void free joint. Mode-mixers were used with all fibers except some of the 1.3 μm measurements. There the mode mixer was removed to obtain more intensity. A block diagram of the experimental set-up is shown in Fig. 4.1.

Fibers were first characterized individually for pulse broadening and then spliced together one-by-one. Measurements of pulse broadening were taken at the end of each fiber. Pulses on

the screen were photographed and then analysed. Problems arose when trying to find the pulse on the scope screen. Propagation velocity through the fiber was unpredictable and sometimes differed by tenths of a microsecond from the individual propagating time.

The pulse-broadening (ΔT) was calculated from the input and output pulse FWHM as follows:

$$\Delta T = [(FWHM_{out})^2 - (FWHM_{in})^2]^{1/2}$$

The dispersion of the fiber is a mixture, chromatic and modal. Total dispersion is given by:

$$T^2(\lambda,L) = T_m^2(\lambda,L) + [T_c(\lambda)L]^2$$

At 1.3 μm $T_c(\lambda) = 0$ thus no correction was required. At .9 μm, $T_c(\lambda)$ was assumed to be constant at .08 nsec/km/nm over the laser bandwidth. Linewidth of the laser was assumed to be 3.3 nm resulting in .264 nsec/km correction to the .9 μm pulse broadening[5] due to chromatic dispersion.

Two engineering rules were deduced from the data:

"p-rule" $T_1(L) = T(L)L^p$

$L = \sum L_n$ = sum of all sections in the link

$T(1)$ = 1 km intercept, determined by fit.

"q-rule" $T_2(L_n) = [\sum T_n^{1/q}]^q$

T_n = P.B. of nth fiber section.

An estimate for T(1) can be obtained by setting

$$T_2(L_n) = T_1(L_n)$$

and

$$p = q = r$$

and obtaining:

$$T(1) = \left[\frac{\left\langle T_n^{1/r}}{\left\langle L_n}\right.\right]^r \qquad (1)$$

The least squares fit and graphing were done on a computer.

Concatenated attenuation measurements were done on the last set of fibers to undergo the pulse broadening test. The fibers were already concatenated, thus, all that had to be done was to break each fiber before and after the splice and take readings. The light source was a Burrus-type LED emitting at 840 nm wavelength. It was powered by a variable (0-30 V DC) voltage source connected in series with a 250 ohm resistor, simulating a constant-current source. A solar cell detector, as used in the temperature cycling tests, provided light intensity readings. Fiber ends were cleaved to avoid scattering the output light. In this way both fiber attenuation and splice loss could be calculated.

4.3 Results

Test results for fibers from four different manufacturers are shown in Figs. 4.2 through 4.8. Both wavelengths are shown for each set, except for the third set, for which only the .84 μm wavelength data was considered because of high attenuation at 1.3

μm. The plots are log-log and show p-rule fit, q-rule fit, as well as the data. Large R shows the closeness of fit for each rule.

The dotted line is drawn for comparison to the fitted data. It is the result of setting p = .7, calculating T(1) from Equation 1 (using T_n's measured for each individual fiber) and using them in the p-rule to compare the prediction to data obtained by measurement. The main area of interest was in the 5 to 10 km range.

Table 4.1 shows three values of the 1-km pulse-broadening (i.e., pulse-broadening for the link extrapolated down to an equivalent of 1 km pulse-broadening). $T_1(1)$ is the result of calculating T(1) from Equation 1 with r = p , where p is obtained from the slope of the fitted curve (shown on each graph) and T_n's are calculated from individual measurements of the fibers. $T_2(1)$ is the result of the same calculation but with r = .7, simulating the calculation a system designer would make lacking concatenation data but knowing the P.B of the fibers to be used.

$T_3(1)$ is the result of the least squares fit to the data (done by computer) and can be read off the graphs.

P is the slope of the p-rule curve fitted to the graphs and should be compared to a p-value at 10 km. At .9 μm the predicted slope is greater than the slope of the fitted p-rule.

Figure 4.6 shows the data for the third set of fibers at .9 μm. A 1.3 μm measurement was not feasible because of high attenuation and equipment problems at this wavelength. The predicted behaviour of this link is overestimated by a small amount. The p-rule gives a better fit than the q-rule but not by as great a margin as for the other sets of fibers.

Figures 4.7 and 4.8 show data for the fourth group of fibers tested. The .9 μm wavelength data is interesting as it shows a drop in pulse broadening between the third and fourth points as well as erratic behaviour between 6 and 10 km, i.e. the two intervals with no increase in pulse broadening. Predicted pulse broadening is drastically overestimated, 4 ns at 10 km as opposed to the measured value at .7, being the engineering rule approximation.

Figures 4.2 and 4.3 show the results for the first set of fibers at .9 and 1.3 μm wavelengths respectively. The fitted p-rule approximates more closely the measured data at 1.3 μm than at .9 μm (R = .997 at 1.3 μm as opposed to .983 at .9 μm), and for both graphs the p-rule is a better fit than the q-rule. The p-rule engineering approximation though is overoptimistic in both cases with the 1.3 μm being drastically underestimated (4 nsec at 10 km predicted versus 9 nsec measured).

Figures 4.4 and 4.5 present data for the second set of fibers, from a different manufacturer than the first. Again, the p-rule gives a better fit to the measured data than the q-rule,

at both wavelengths. But the p-rule at .9 μm gives a better fit than the p-rule at 1.3 μm. The predicted behaviour (dotted line) gives a good approximation but underestimates the pulse broadening by less than 2 nsec for 10 km. The 1.3 μm data behaves more reasonably, giving a good fit to the p-rule. The slope is underestimated by the prediction but the disparity at 10 km is small.

In general the p-rule gives a better fit to the data than the q-rule and, except for two cases, the predicted values of pulse broadening at 10 km are within 2 nsec of the measured value. The two exceptions show that the predicted values can vary up to 100% at 10 km. Previous results show a good fit to measured data using the p-rule as well.

The concatenated attenuation behaviour was as expected, i.e., the individual attenuation values of the fiber add linearly with the splice loss, accounting for the total attenuation. The results are shown in Table 4.2; fiber attenuation was calculated from intensity readings at the beginning and end of the fiber, splice loss was calculated from the intensity readings before and after the splice. The total attenuation was calculated from the intensity at each point and at the beginning of the concatenated fiber. The average splice loss was .3 db.

4.4 Conclusions

The p-rule gives a better fit to the data than the other

rules tried. This seems to hold true in general.

A system designer, given data on individual fibers, can estimate the pulse broadening and attenuation of a link with reasonable confidence in the results (as a rule, p = .7 gives undervalued pulse broadening at 10 km). Raising the p-value to .8 would give a higher safety margin.

Further experiments should be done to determine the exact cause of the reduced pulse broadening. A long fiber (preferably 6-8 km) should be characterized as to attenuation and pulse broadening, then broken into shorter (1 km or less) pieces and concatenated as described in this Chapter. This experiment would reveal whether or not the splices are causing the decreased pulse broadening.

ICE CRUSH TEST

Cable 4

Increase in attenuation with temperature with water in the core, db/km.

No. of pipes (crush pts.)	Fiber	Total atten.	Less cable atten.	Atten/cp.	Temp.
	0	.30	.14	.07	
1	W	.12	.17	.09	-11
	B	.27	.36	.13	
	0	.41	.26	.07	
2	W	.12	.18	.04	-9
	B	.45	.53	.13	
	0	.40	.25	.06	
3	W	.11	.17	.03	-10
	B	.45	.53	.09	
	0	.58	.43	.04	
6	W	.14	.20	.02	-11
	B	.70	.80	.07	
	0	1.8	1.4	.12	
6	W	.68	.54	.05	-37
	B	1.68	1.4	.12	
	0	.43	.06	.01	
6	W	.18	.03	.00	+64
	B	.46	.16	.01	

Table 2.1

PULL TEST

Table of changes in attenuation during pull test on cable 3. db/km.

Tension (lbs)	Time (hrs)	B	Fibers 0	G
505	.0	+.77	+.76	+.81
505	.5	+.66	+.62	+.71
0	.0	-.03	+.15	+.01
0	.5	-.17	+.11	-.01
760	.0	+1.4	+1.5	+1.4
760	.5	+1.1	+1.4	+1.3
0	.0	-.17	+.06	+.15
0	.5	-.10	-.00	+.17
915	.0	+2.5	+1.9	+2.7
915	.5	+2.0	+1.8	+1.6
0	.0	+0.4	+.26	+.09
0	.5	-1.8	+.11	-.11
1090	.0	-.10	+2.7	+2.1
1080	.5	+.81	+2.4	+1.5
0	.0	-1.2	+.03	-.27
0	.5	-1.4	-.04	-.30
Final attenuation		+3.0	+5.5	+3.0

Table 2.2

1 KM INTERCEPT

Table of 1 kilometer intercept of pulse broadening, predicted and fitted to concatenation data. nsec/km.

$T_1(1)$ Calculated	P	$T_2(1)$	T_3 (fitted)	Fiber
1.25	.77	1.3	1.26	1
.660	.97	.75	.95	2
1.12	.65	1.1	1.37	3
1.88	.79	2.0	1.97	4
1.05	.65	1.0	.97	5
.833	.58	.81	.45	6
.678	.92	.69	.48	7

Table 4.1

CONCATENATED ATTENUATION

Fiber Attenuation	Splice Attenuation	Total Attenuation
	.37	.37
3.87		4.2
	.15	4.4
2.19		6.6
2.76		9.8
	.24	10.0
2.49		12.5
3.20		15.8
	.24	16.1
2.76		18.8
	.30	19.1
3.25		22.4
	.00	22.4
2.50		24.9
	.92	25.8
2.89		28.6
	.22	28.9
2.51		31.4

Table 4.2

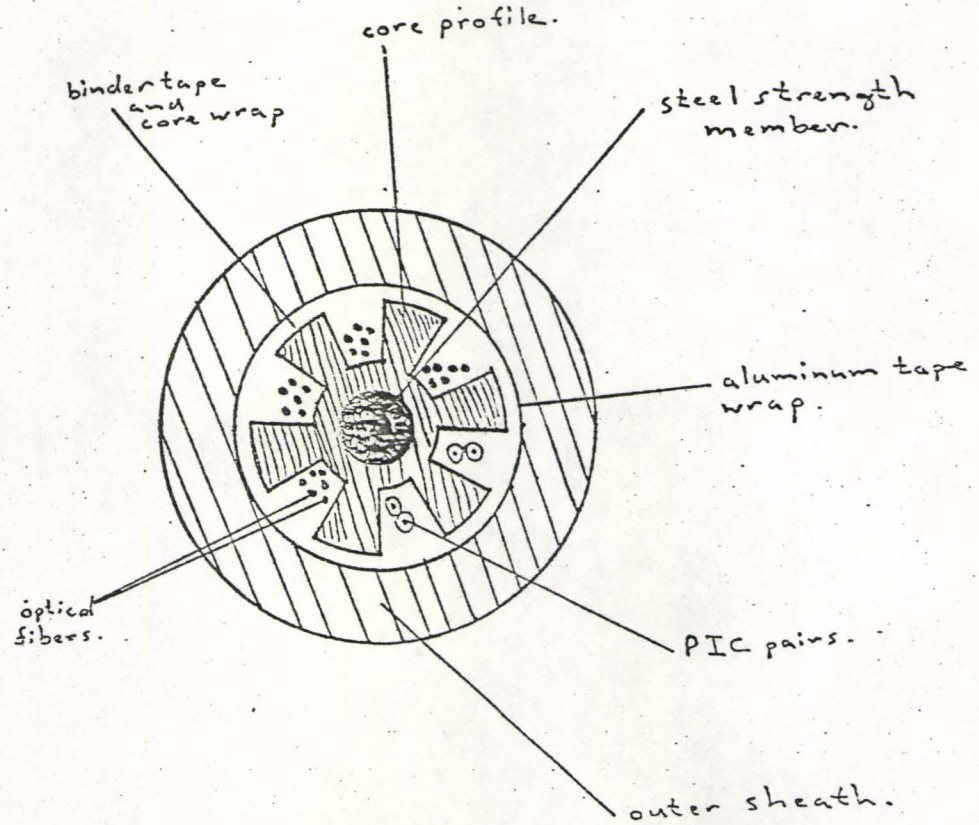

Fig. 2.1 Cross Section of 6 slot cable containing 24 fibers and 2 PIC pairs.

Fig. 2.2 Water ingress and ice crush test device.

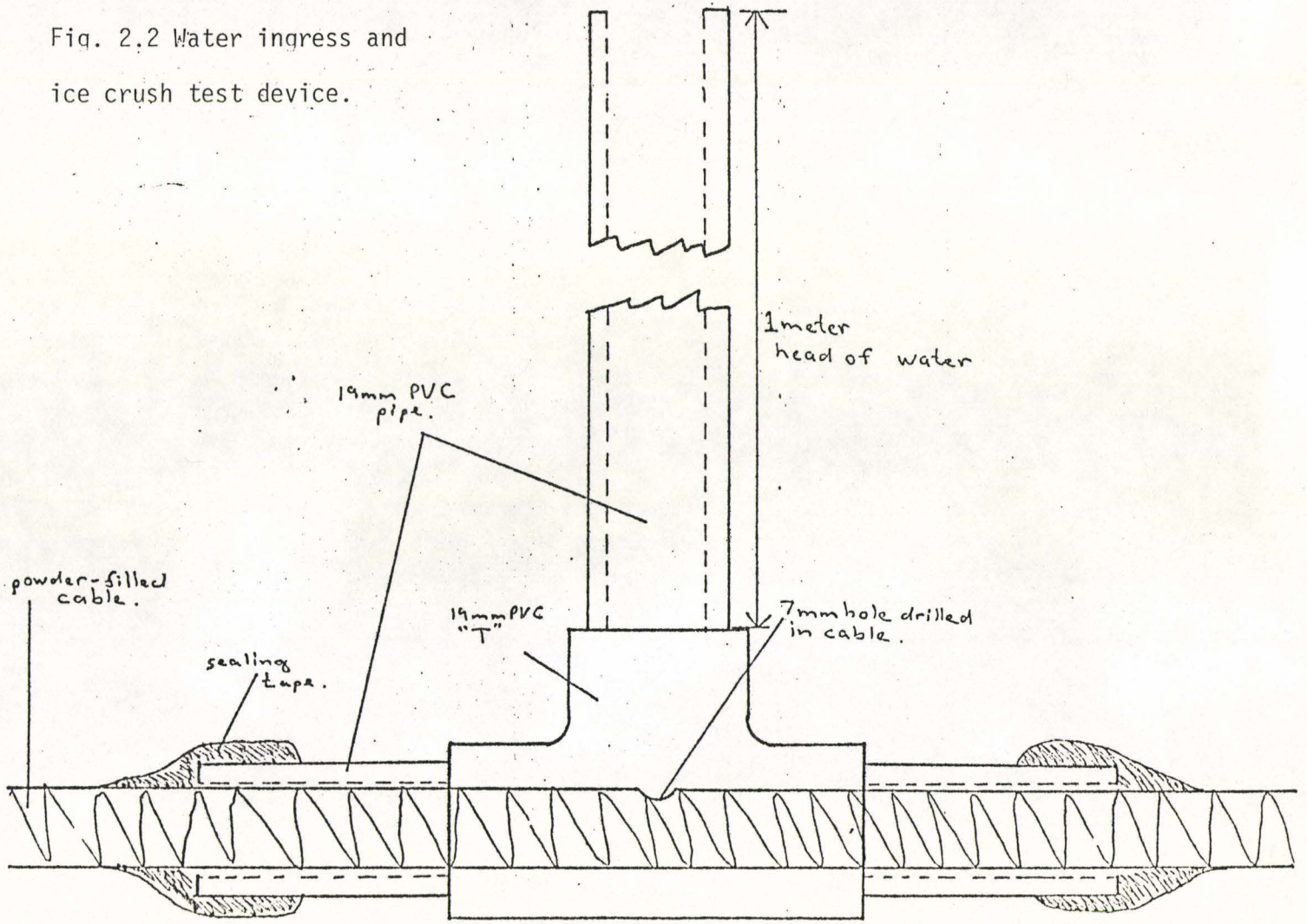

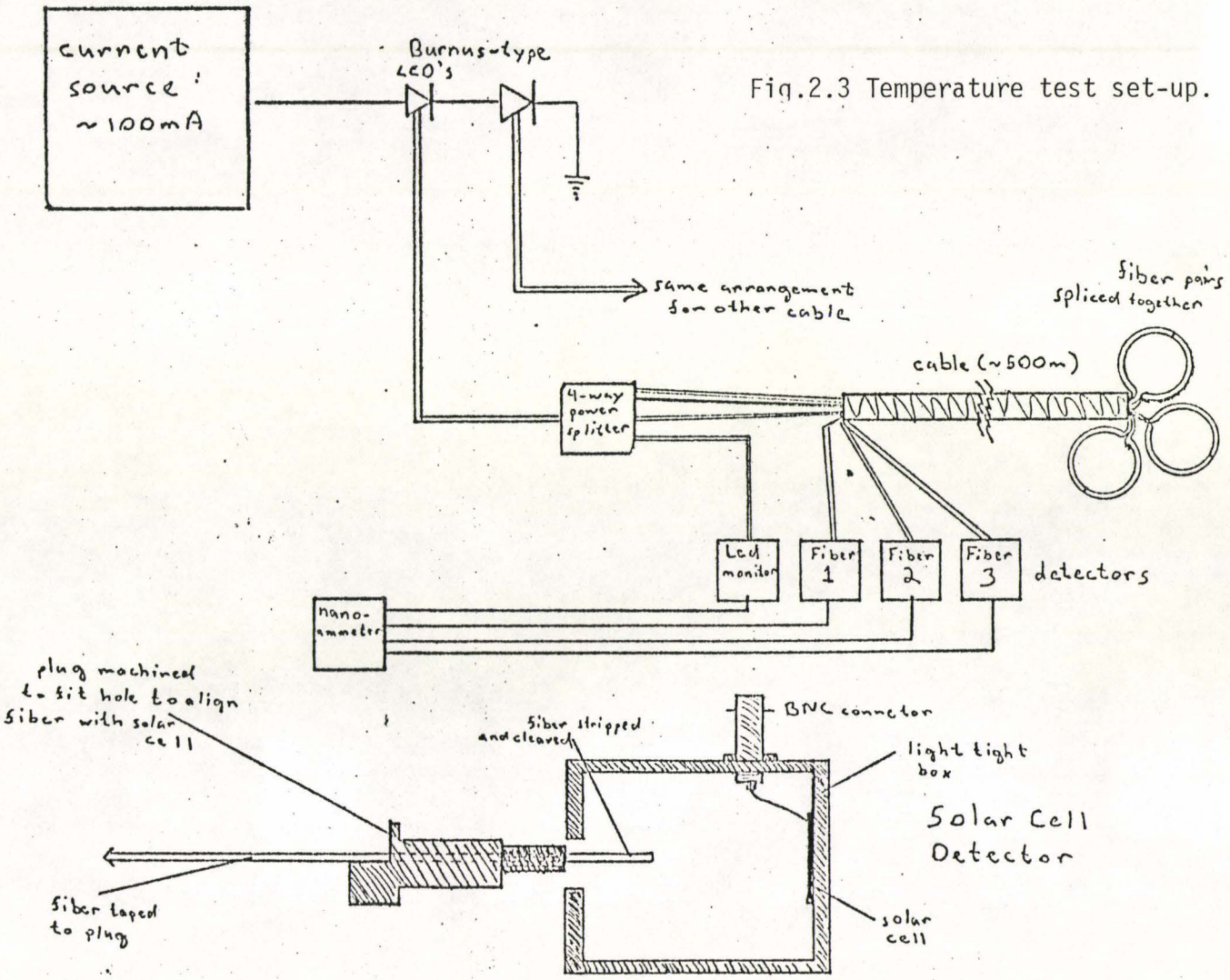

Fig.2.3 Temperature test set-up.

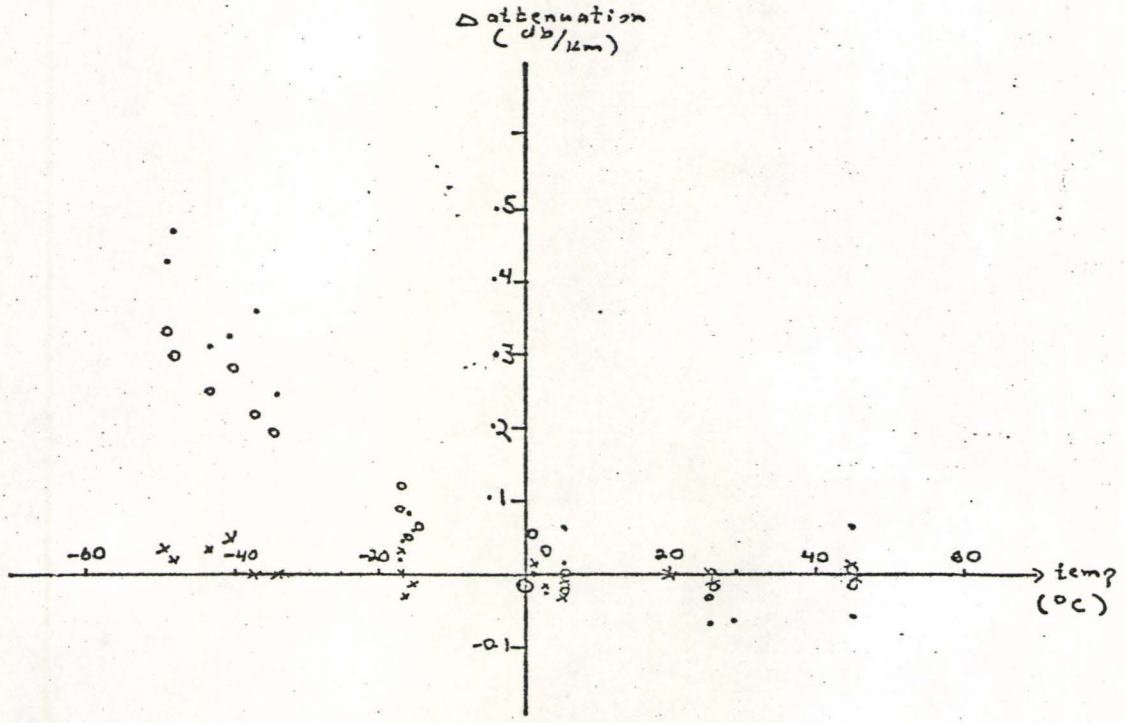

Fig. 2.4(a)

Cable 1

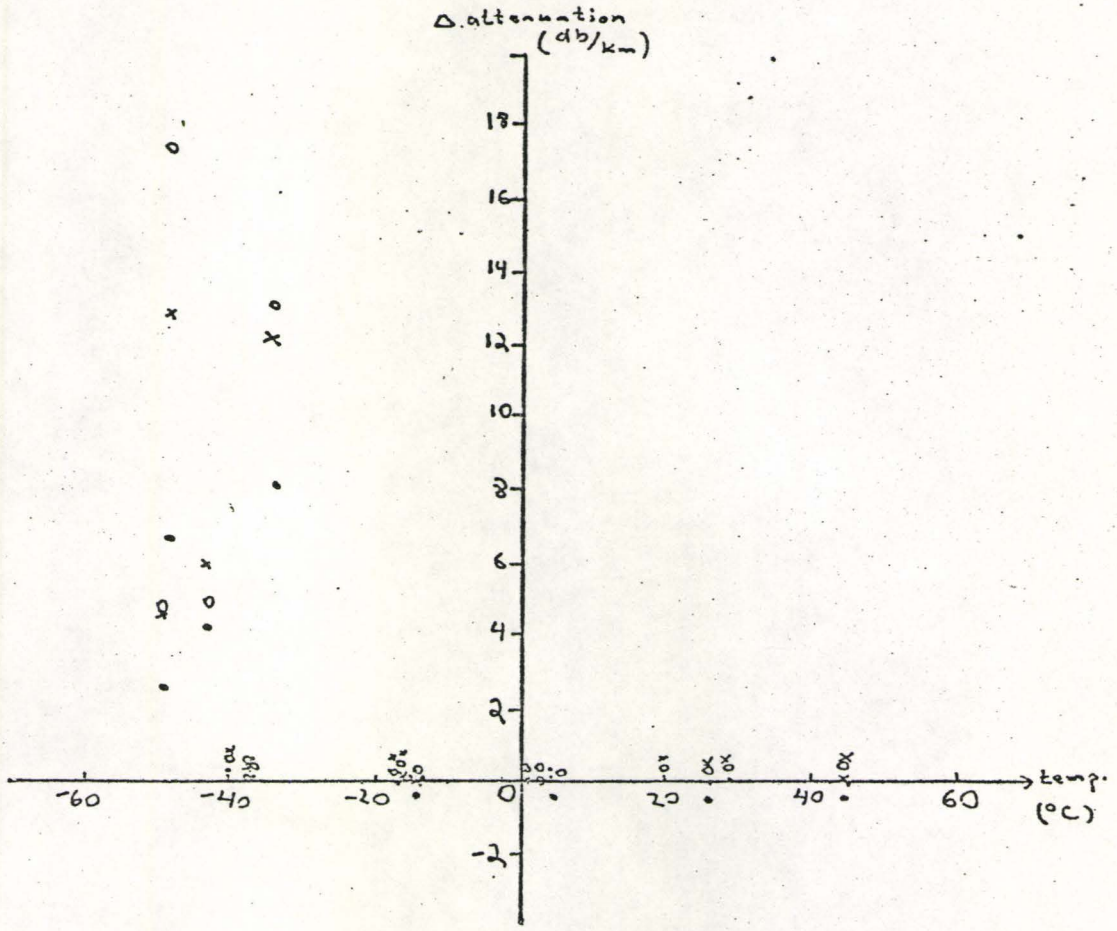

Fig. 2.4(b)

Cable 2

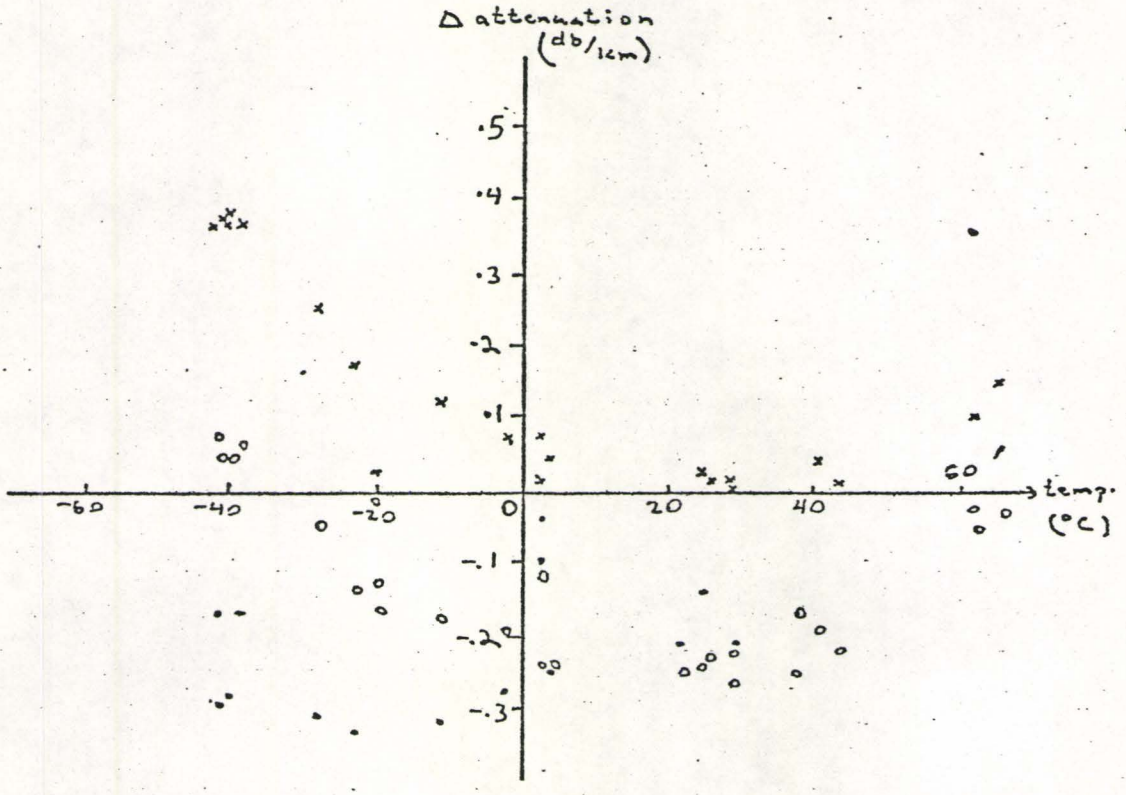

Fig. 2.4(c)

Cable 3

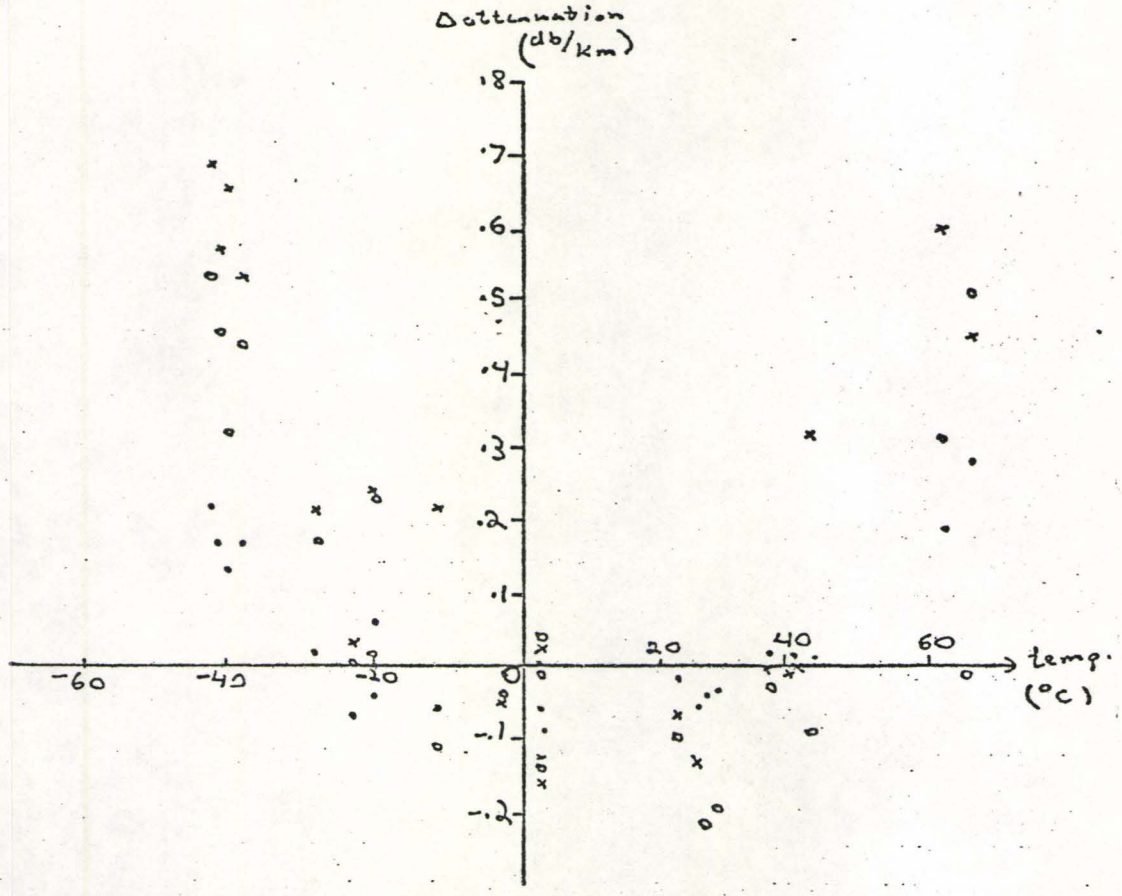

Fig. 2.4(d)

Cable 4

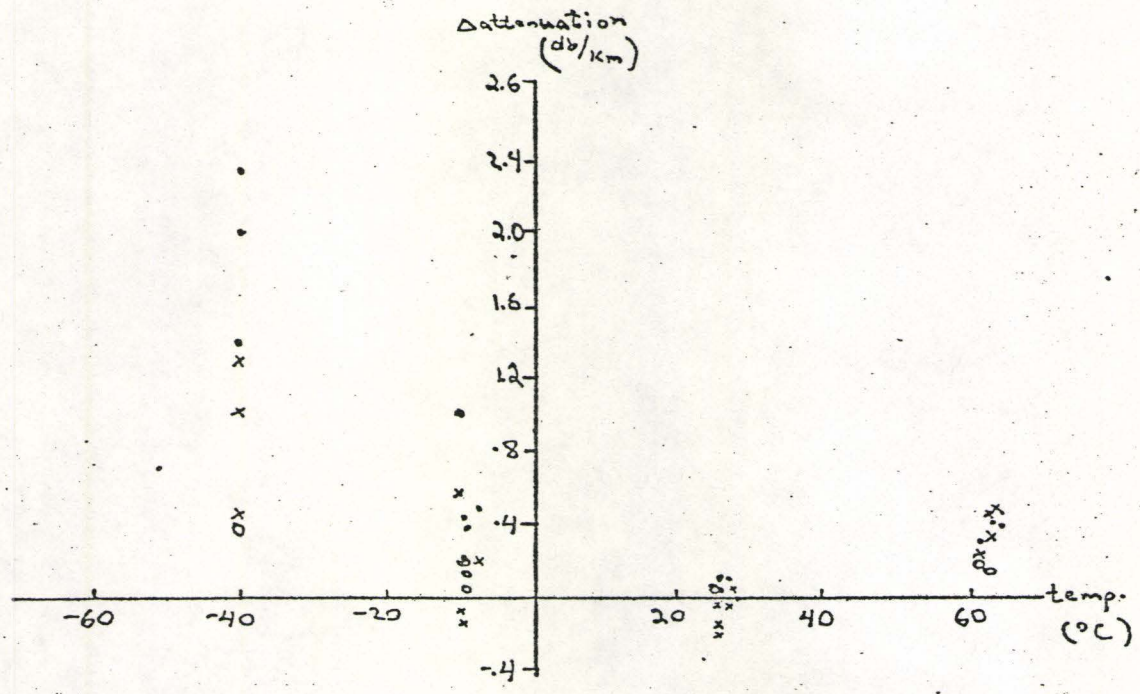

Fig. 2.4(e)

Cable 5

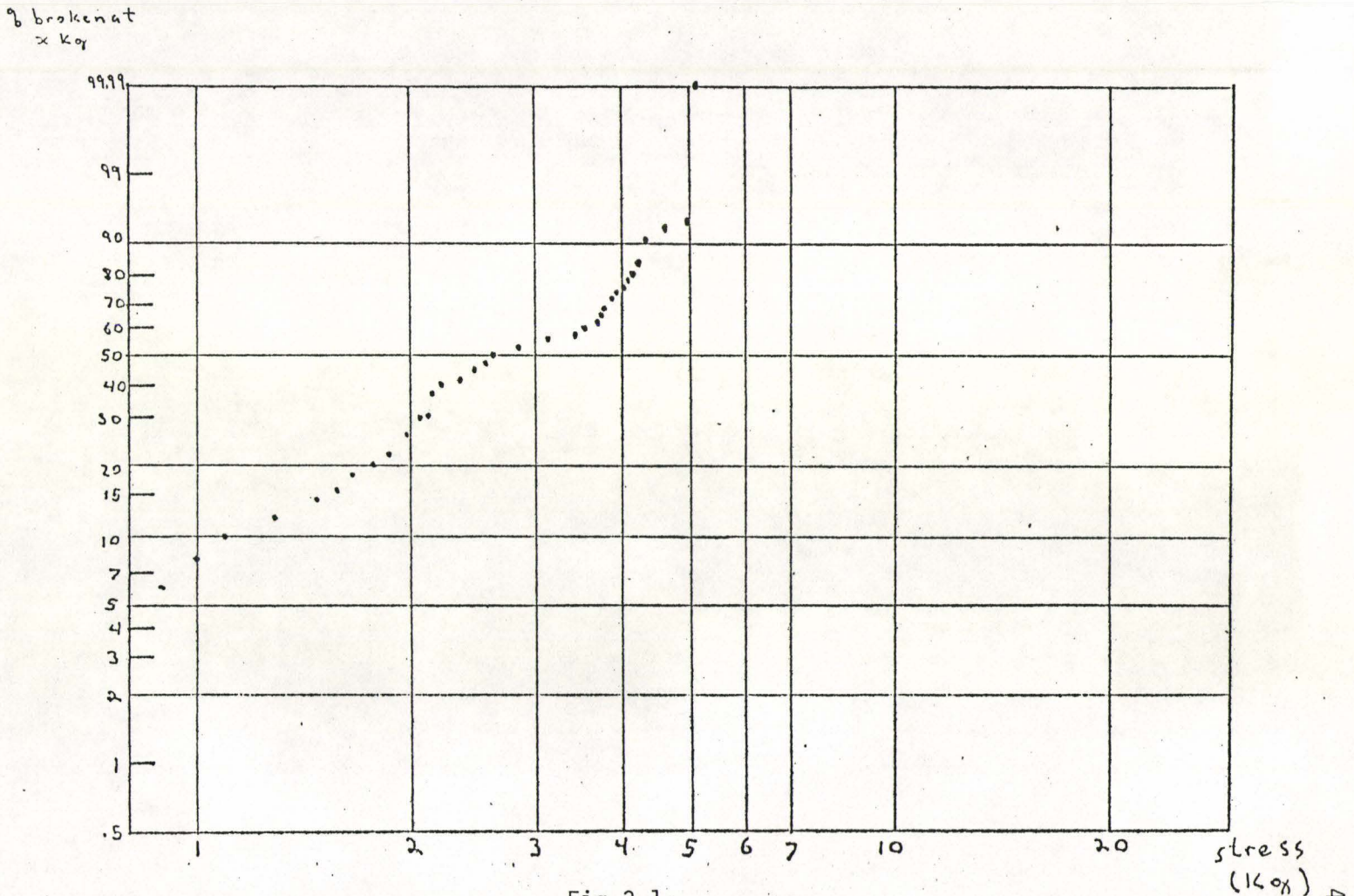
% broken at
x ksi
99.99
99
90
80
70
60
50
40
30
20
15
10
7
5
4
3
2
1
.5
1
2
3
4
5
6
7
10
20
stress
(ksi)

Fig 3.1

% broken
at x kg.

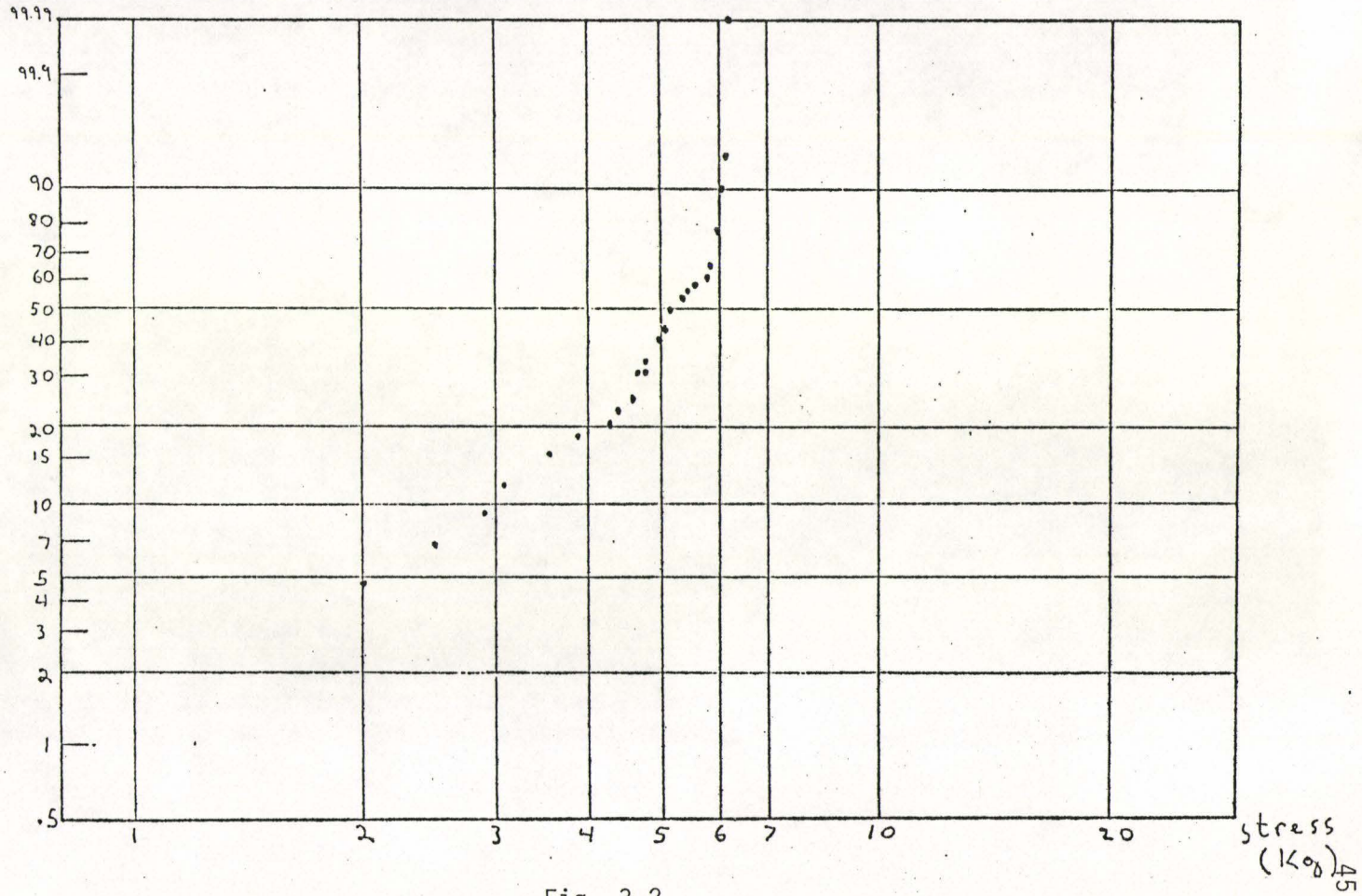

Fig. 3.2

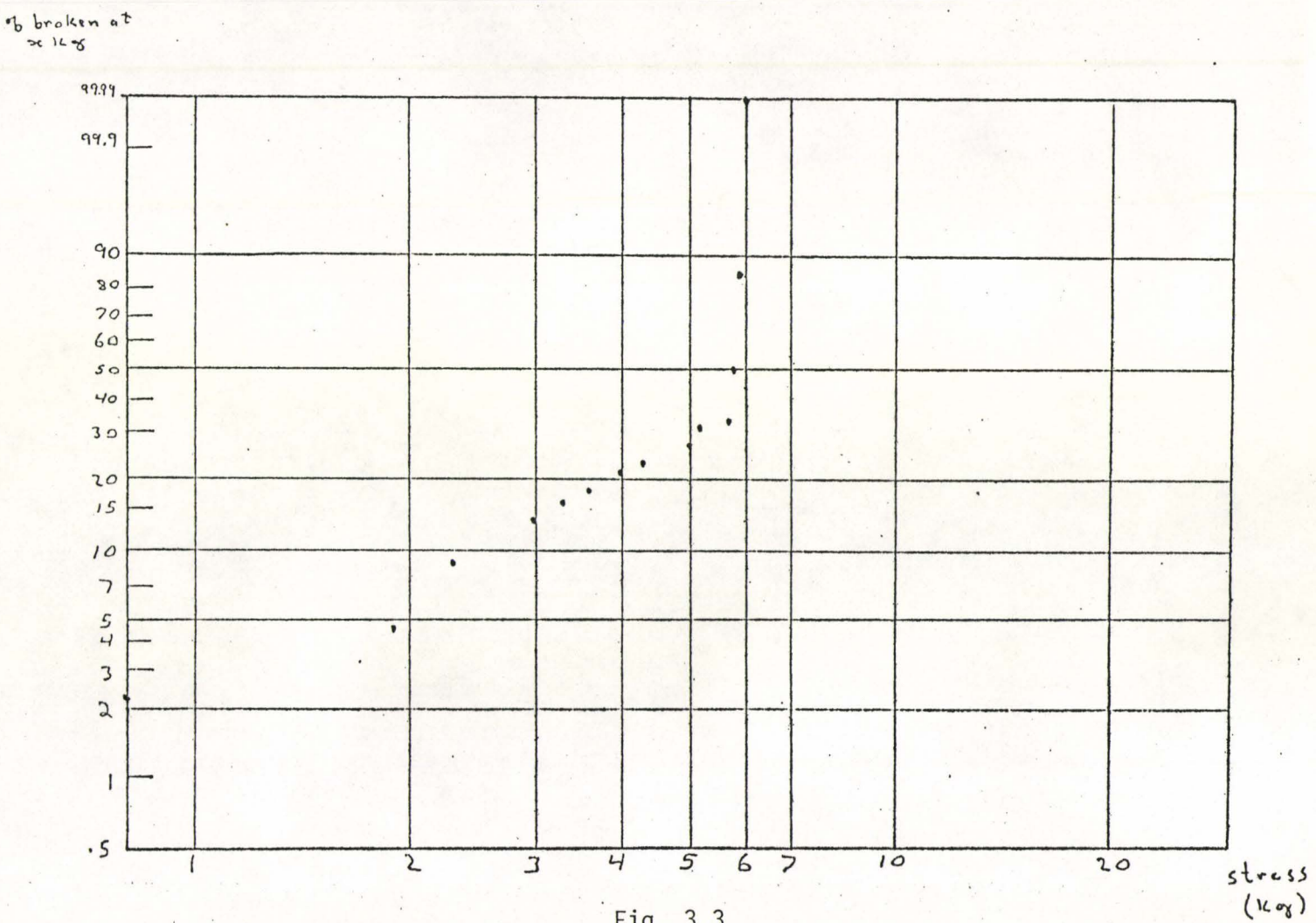
% broken at
stress
(kg)
99.99
99.9
90
80
70
60
50
40
30
20
15
10
7
5
4
3
2
1
.5
1
2
3
4
5
6
7
10
20

Fig. 3.3

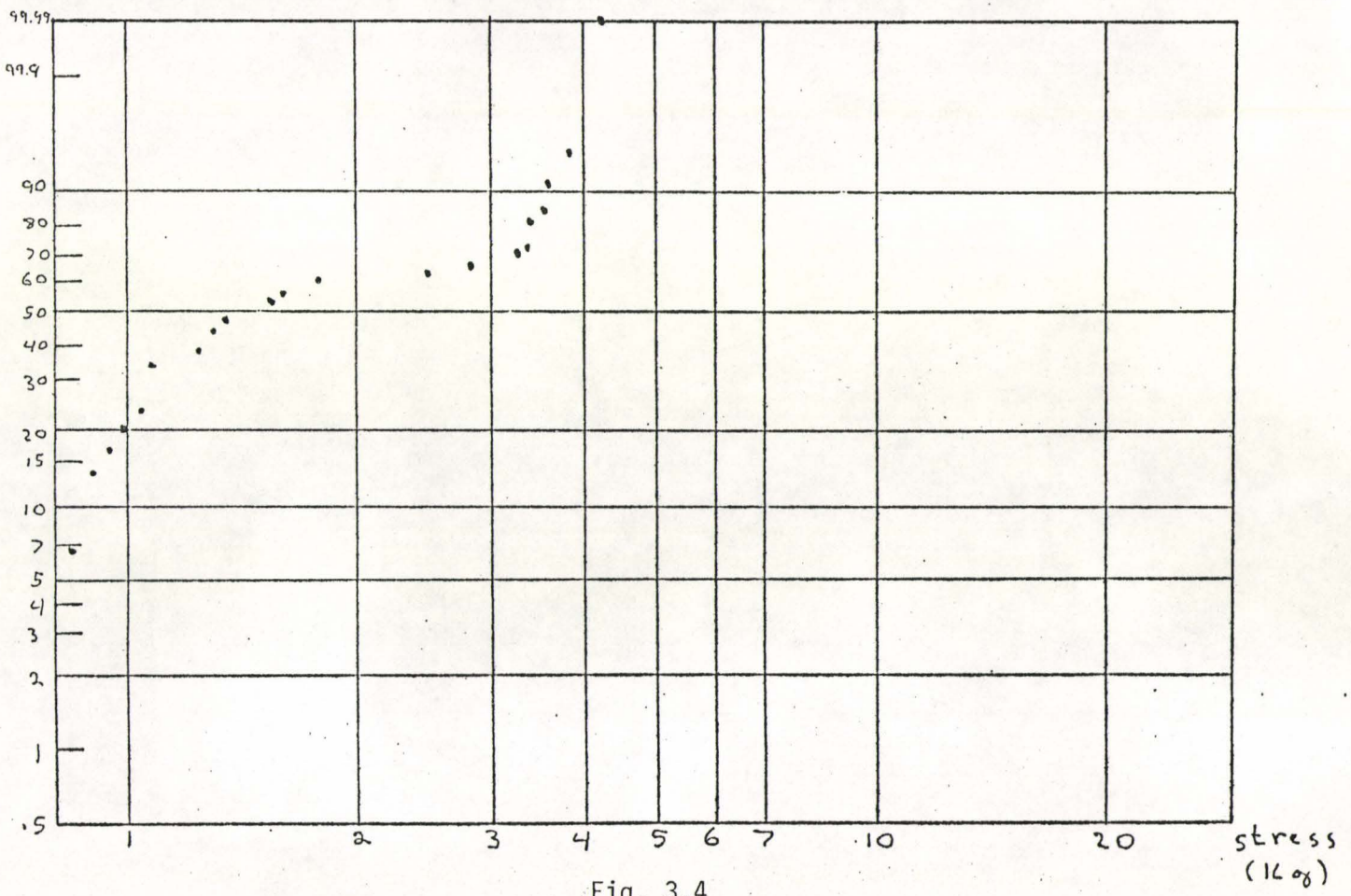
η_b broken at
x log.
99.99
99.9
90
80
70
60
50
40
30
20
15
10
7
5
4
3
2
1
.5
1
2
3
4
5
6
7
10
20
stress
(log)

Fig. 3.4

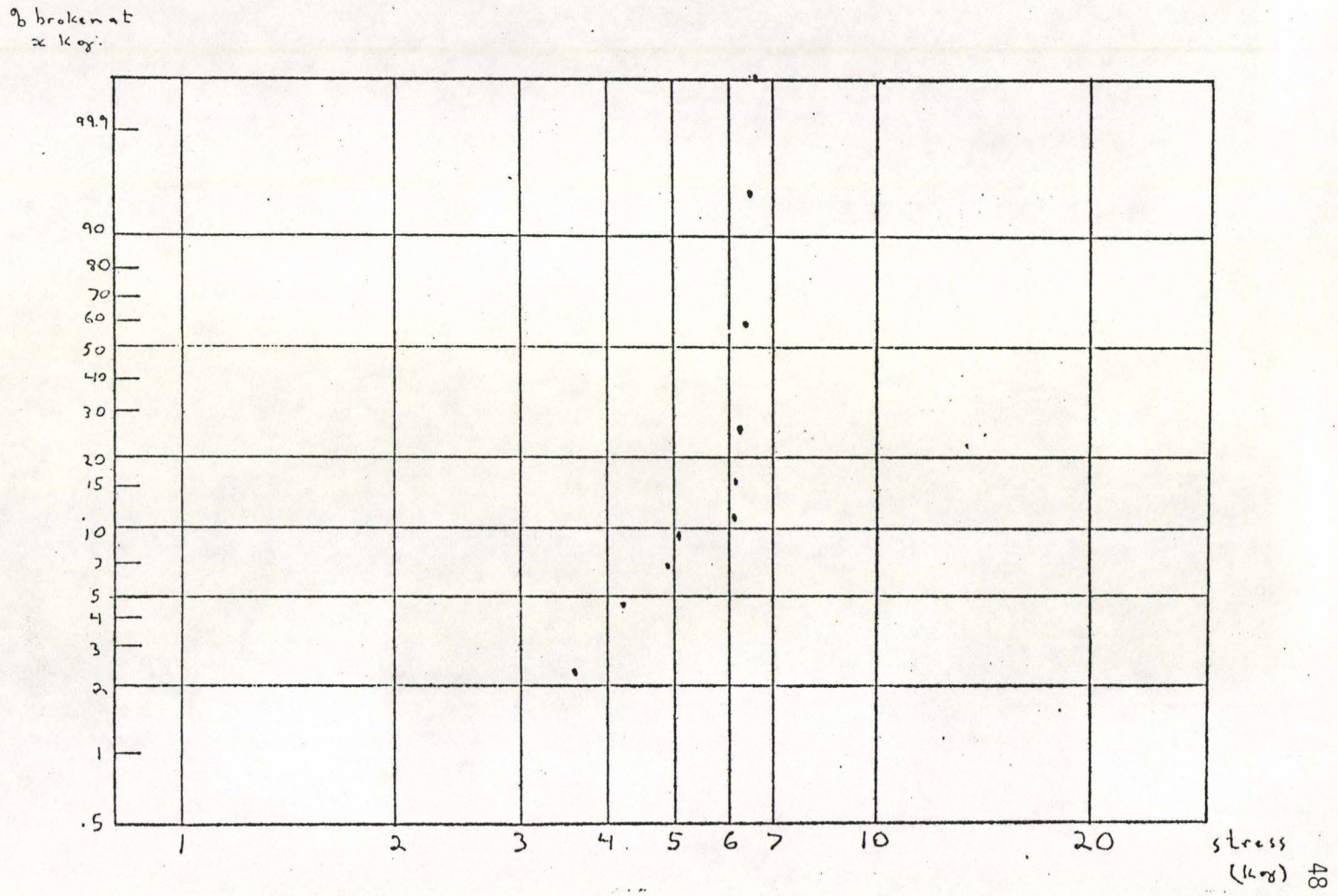
% broken at
x kgf.
99.9
90
80
70
60
50
40
30
20
15
10
7
5
4
3
2
1
.5
1
2
3
4
5
6
7
10
20
stress
(kgf)

Fig. 3.5

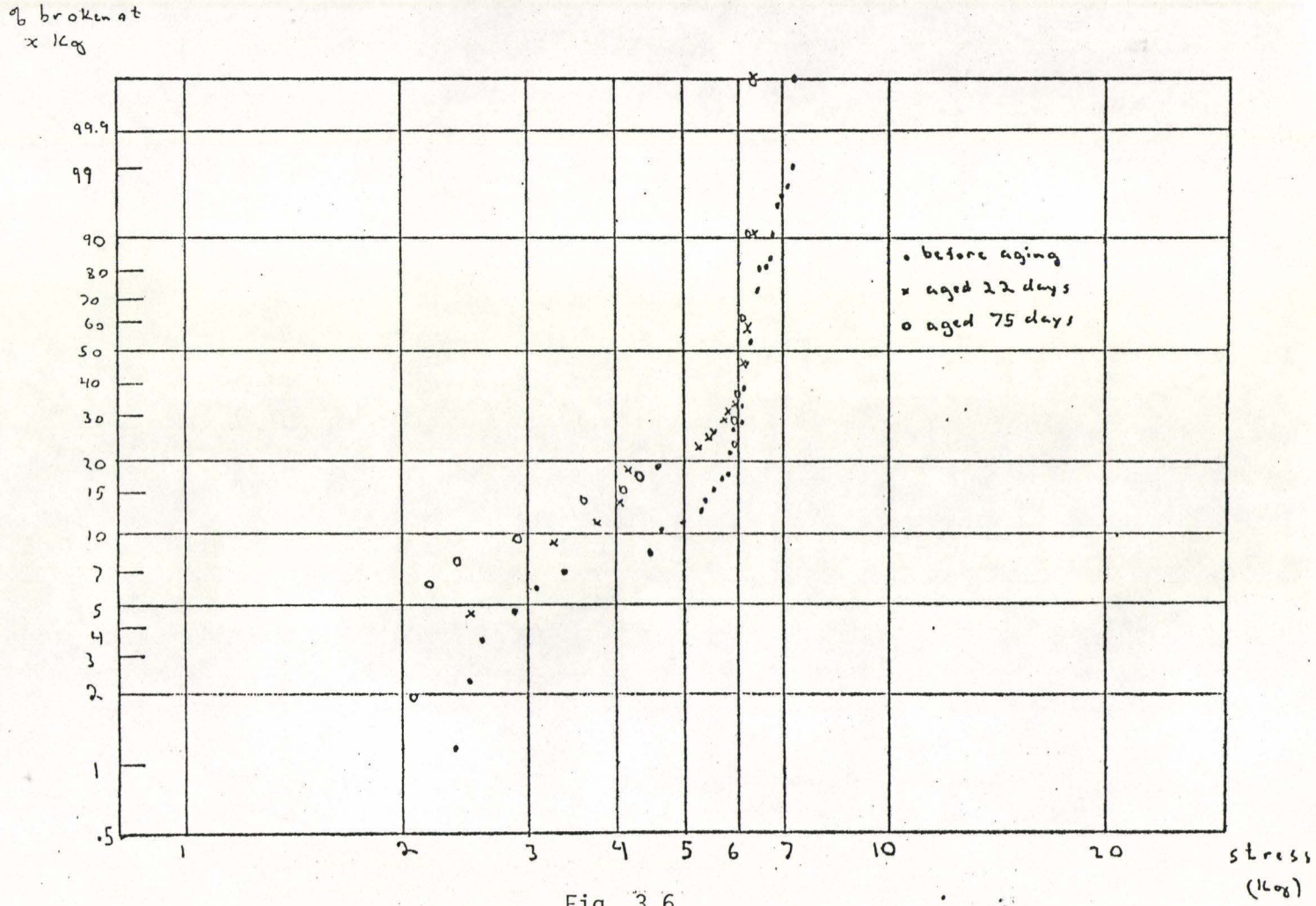
% broken at
x 1Cg
99.9
99
90
80
70
60
50
40
30
20
15
10
7
5
4
3
2
1
.5
1
2
3
4
5
6
7
10
20
stress
(1Cg)
• before aging
x aged 22 days
o aged 75 days

Fig. 3.6

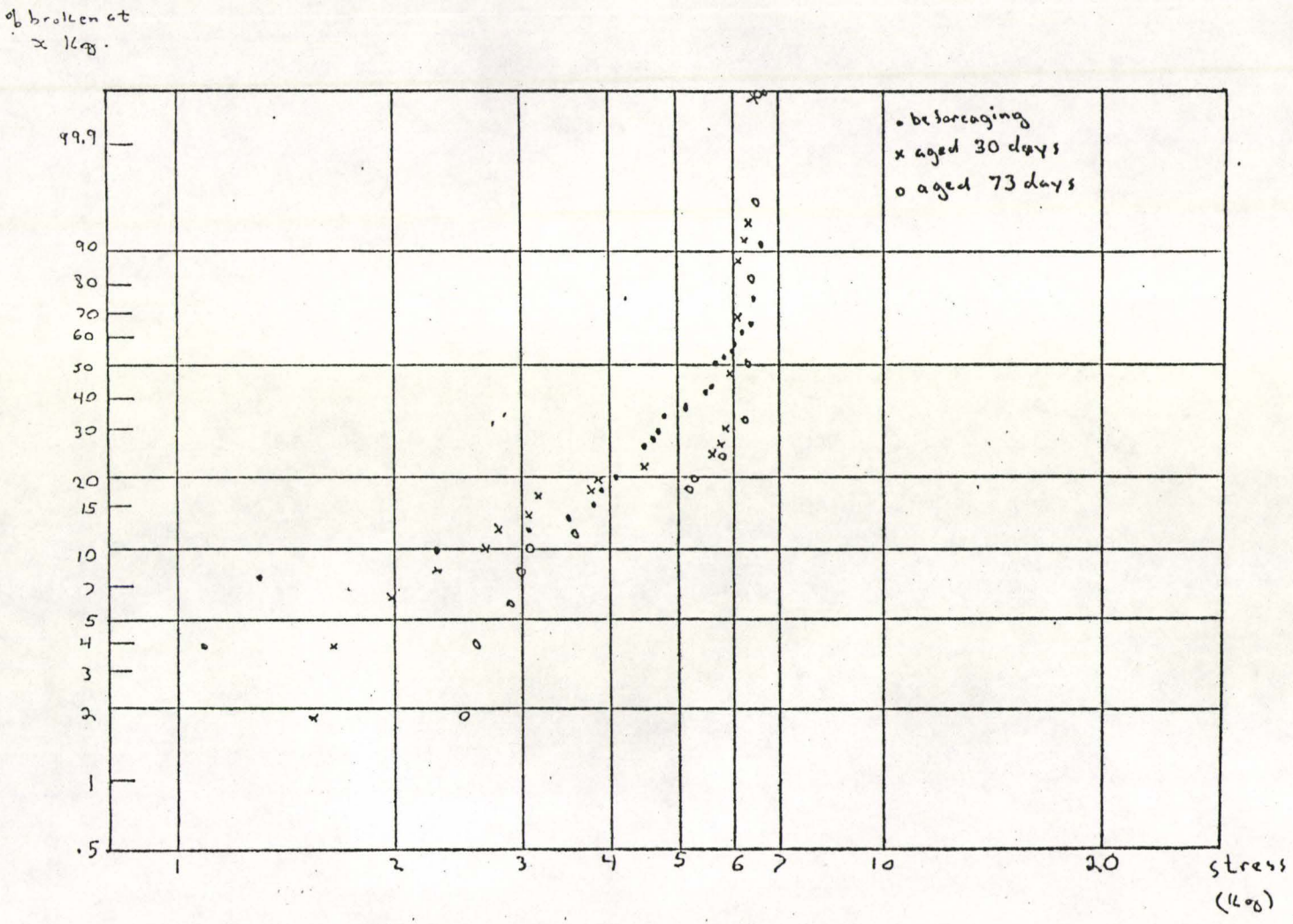
% broken at
x log.
99.9
90
80
70
60
50
40
30
20
15
10
7
5
4
3
2
1
.5
1
2
3
4
5
6
7
10
20
stress
(log)
• before aging
x aged 30 days
o aged 73 days

Fig. 3.7

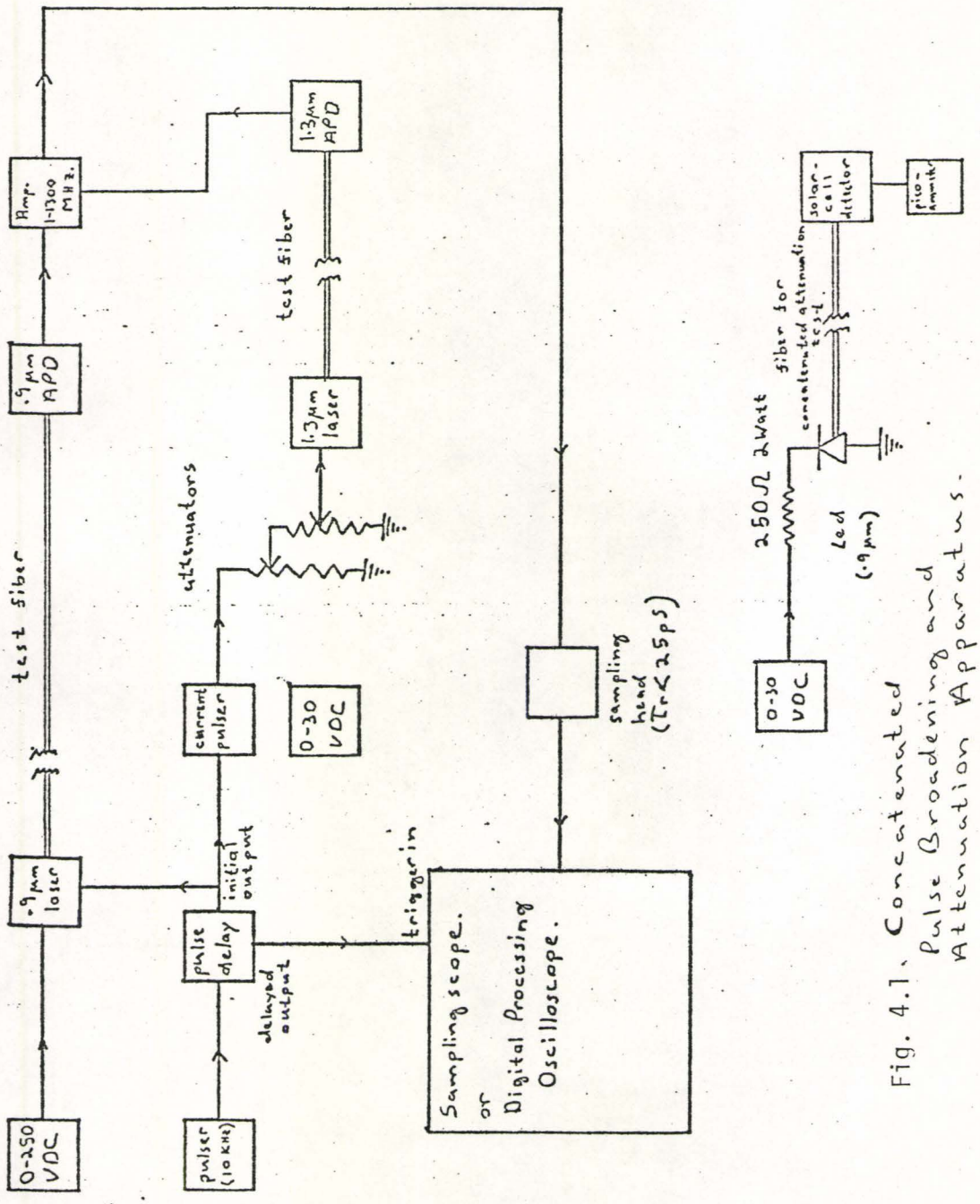

Fig. 4.1. Concatenated Pulse Broadening and Attenuation Apparatus.

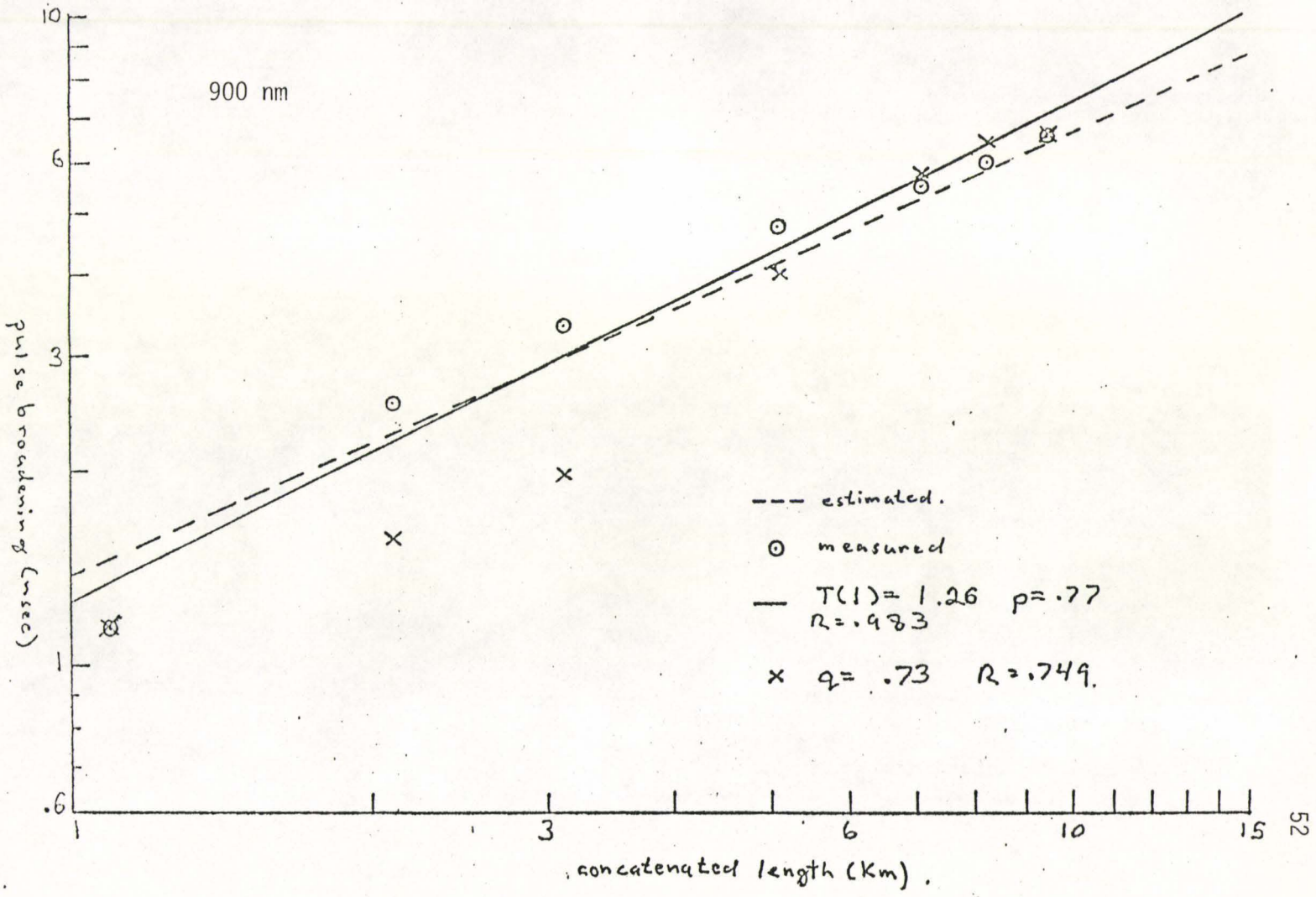
900 nm
pulse broadening (nsec)
10
6
3
1
.6
1
3
6
10
15
concatenated length (Km).
--- estimated.
measured
T(1)= 1.26 p=.77
R=.983
× q= .73 R=.749.

Fig. 4.2

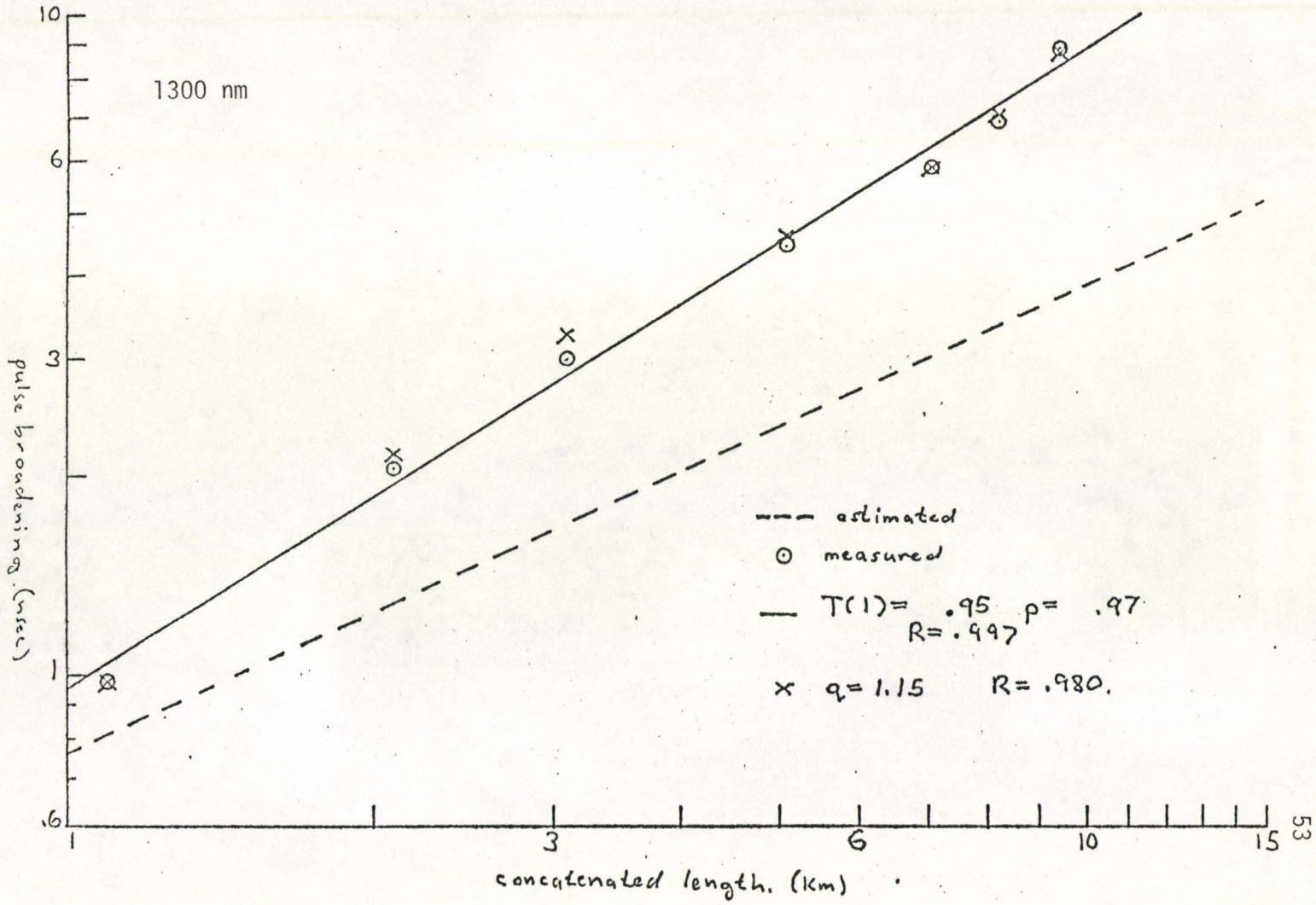
10
6
3
1
.6
1300 nm
pulse broadening (nsec)
--- estimated
⊙ measured
— T(1)= .95 ρ= .97
R= .997
× q= 1.15 R= .980.
1
3
6
10
15
concatenated length. (km)

Fig.4.3

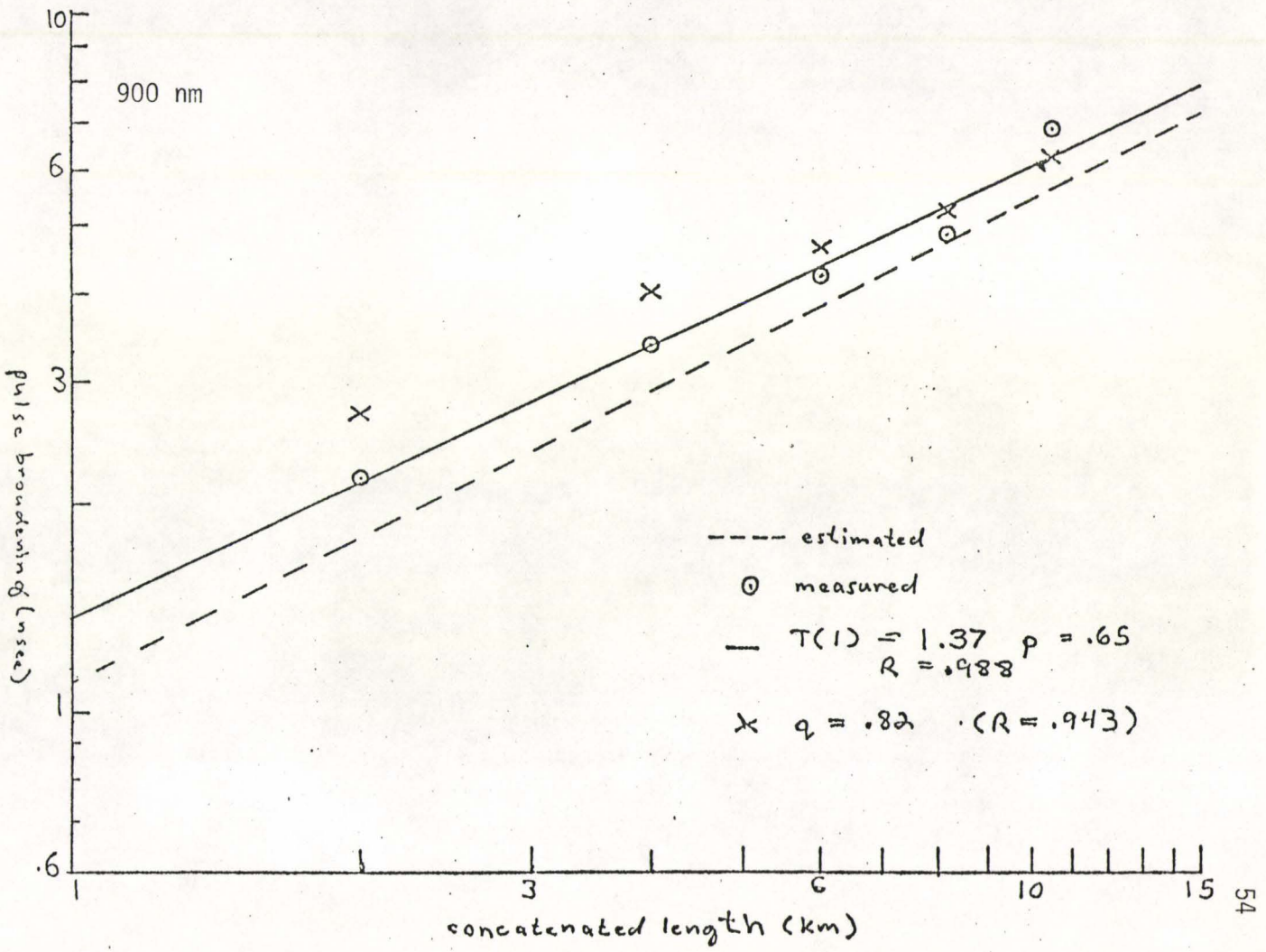
900 nm
10
6
3
1
.6
pulse broadening (nsec)
1
3
6
10
15
concatenated length (km)
---- estimated
⊙ measured
— T(1) = 1.37 p = .65
R = .988
× q = .82 (R = .943)

Fig. 4.4

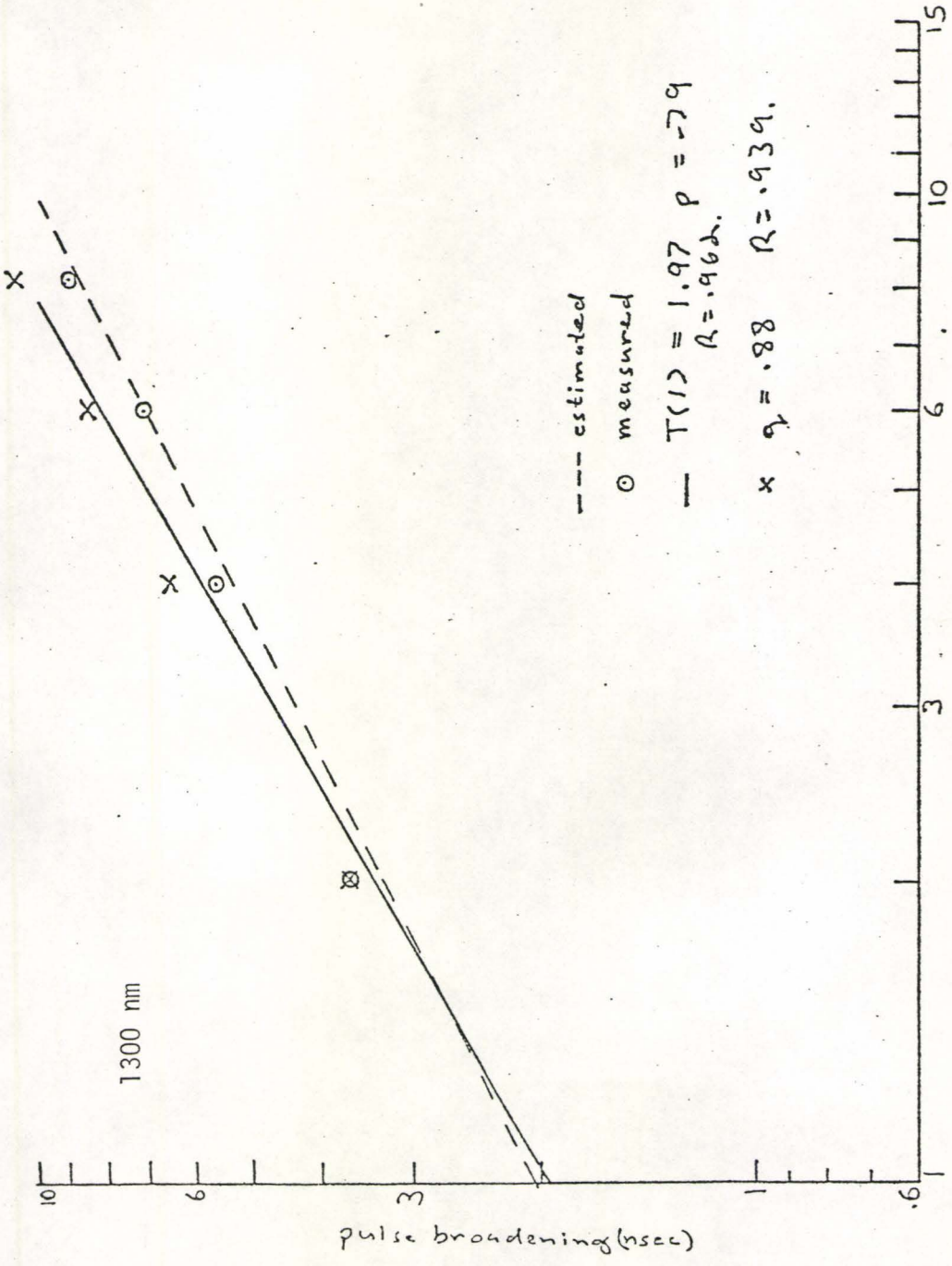
1300 nm
pulse broadening (nsec)
concatenated length (km)
--- estimated
⊙ measured
— T(1) = 1.97 p = .79
R = .962
× q = .88 R = .939
10
6
3
1
.6
1
3
6
10
15

Fig. 4.5

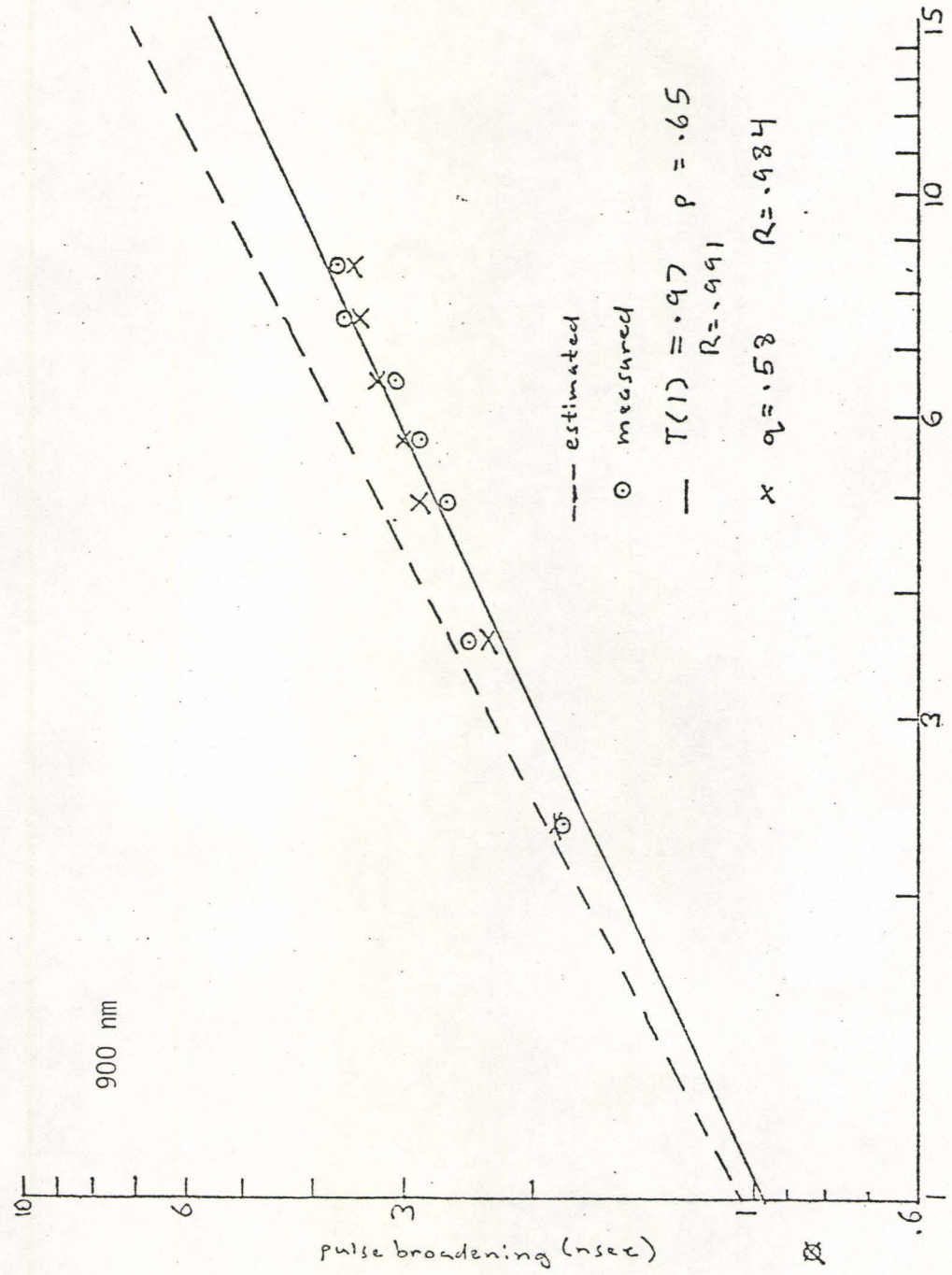
900 nm
pulse broadening (nsec)
10
6
3
1
.6
1
3
6
10
15
concatenated length (km)
--- estimated
⊙ measured
— T(1) = .97 p = .65
R=.991
× q=.53 R=.484

Fig. 4.6

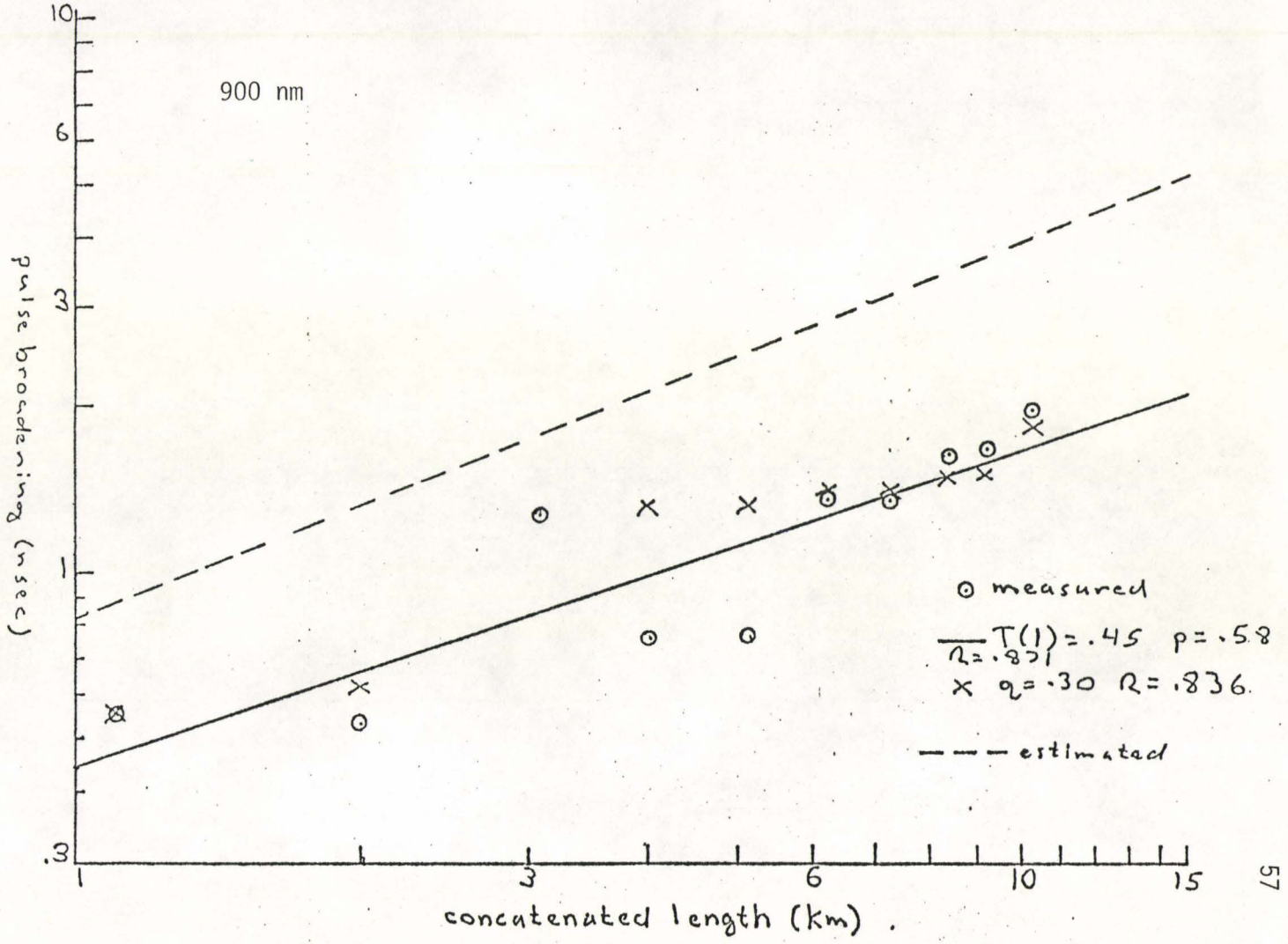
900 nm
pulse broadening (nsec)
10
6
3
1
.3
1
3
6
10
15
concatenated length (km)
⊙ measured
T(1) = .45 p = .58
R = .831
× q = .30 R = .836
— — — estimated

Fig. 4.7

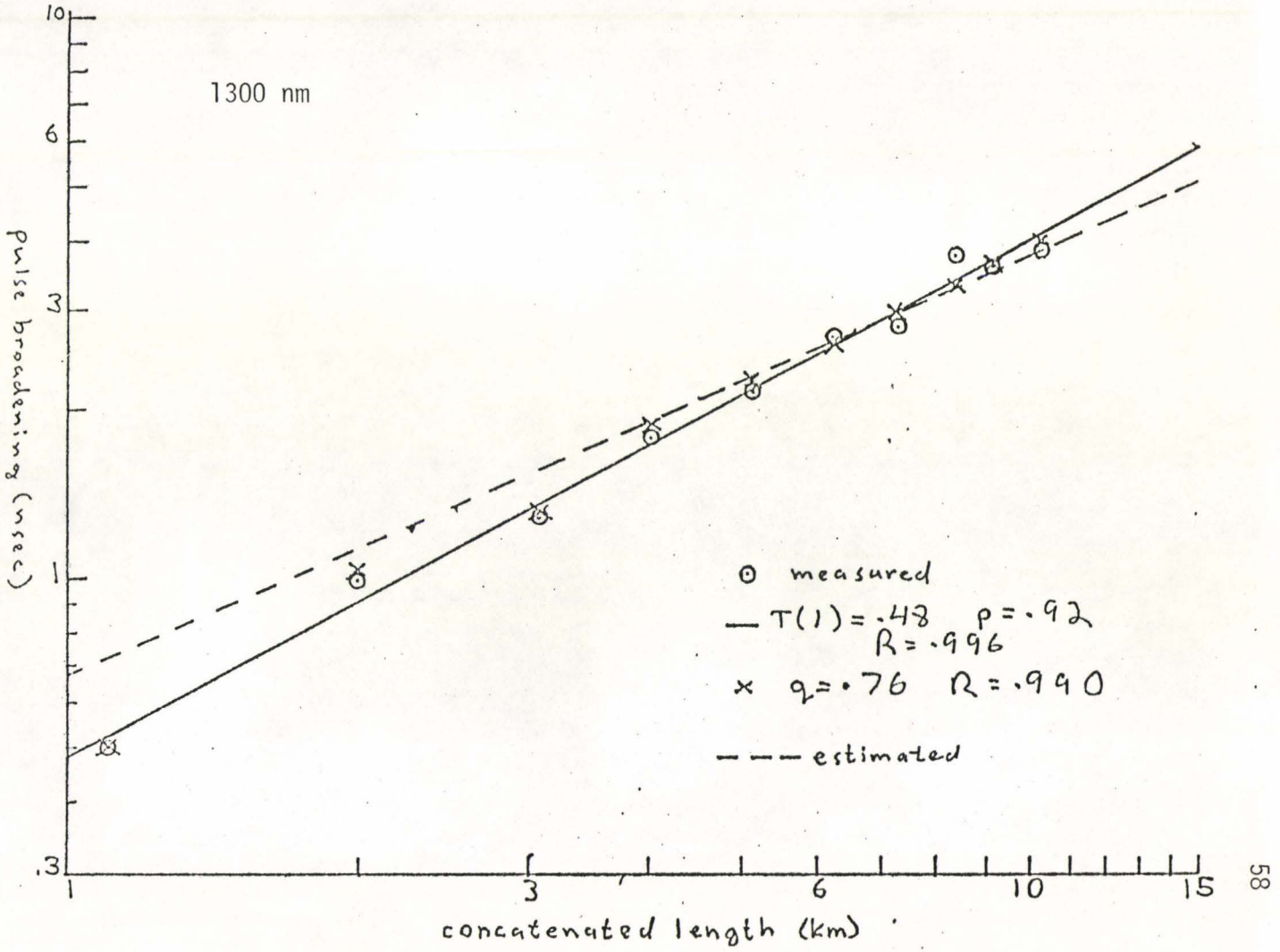
1300 nm
pulse broadening (nsec)
10
6
3
1
.3
1
3
6
10
15
concatenated length (km)
⊙ measured
— T(1) = .48 p = .92
R = .996
× q = .76 R = .990
— — — estimated

Fig. 4.8

REFERENCES

1. Internal memo, Northern Telecom; April 24, 1980, T.S. Swiecicki.

2. Internal memo, Bell-Northern Research Systems Division, November 1979, part 5.

3. Private Communication: C.C. Tan, Dept. 3K34, B.N.R.

4. Internal memo, B.N.R.; June 12, 1980, F.P. Kapron, P. Garel-Jones.

5. Private Communication; F.P. Kapron, B.N.R.

6. Optical Fiber Telecommunications; ed; E. Miller, A.G. Clynoweth; Ch. 12; Fiber Characteristics, Mechanical; D. Kalish, C.R. Kurkijan, B.K. Tariyal, T.T. Wang, pg. 401-433.

7. Effect of Dust on Fiber Strength: Appl. Phys. Lett., Vol. 30, No. 2, Jan. 15, 1977.

8. Private Communication: M. Yataki, B.N.R.